



ORIGINAL ARTICLE

Ultrasonic-assisted-microwave quick synthesis of Pd nanoparticles on N-doped porous carbon for efficient direct hydrogen peroxide synthesis from hydrogen and oxygen at atmospheric pressure



Yongyong Shi ^{a,b}, Donghai Jiang ^{a,c}, Liming Zhou ^{a,c}, Jingyun Zhao ^{a,b}, Jun Ma ^{a,b}, Qian Lin ^{a,b,*}, Hongyan Pan ^{a,b,*}

^a College of Chemistry and Chemical Engineering, Guizhou University, Guiyang, Guizhou 550025, China

^b Guizhou Key Laboratory of Green Chemical and Clean Energy Technology, Guiyang, Guizhou 550025, China

^c College of Chemical Engineering, Guizhou Institute of Technology, Guiyang 550003, China

Received 23 April 2023; accepted 19 June 2023

Available online 24 June 2023

KEYWORDS

Pd catalyst;
Ultrasonic-assisted-microwave;
Quick synthesis;
N-doped porous carbon;
The direct synthesis of H₂O₂ from H₂ and O₂

Abstract Directly synthesizing H₂O₂ from H₂ and O₂ at atmospheric pressure requires a highly efficient Pd catalyst, which poses a challenge for reasonable design and simple synthesis of Pd catalyst. In this study, a series of Pd/NPCS catalysts were synthesized by various methods with mono-disperse, uniform-size and N-doped porous carbon sphere named NPCS as the support and PdCl₂ as the palladium precursor. The results indicated that the ultrasonic-assisted-microwave quick synthesis method significantly reduced the synthesis time of Pd catalyst. The Pd nanoparticles obtained via this method were well-distributed on the NPCS support, with a smaller particle size, a narrower particle size distribution range, and more exposed Pd active sites, which leading to improved H₂O₂ generation rate compared to traditional preparation methods. Additionally, N-doped, high specific surface area, and abundant mixed micro-mesoporous pore structure of NPCS support improved the transfer and diffusion performance of Pd/NPCS catalysts, facilitating the adsorption of reactants and desorption of H₂O₂ from Pd active sites, and effectively inhibited hydrogenation and decomposition side reactions caused by the breaking of the O-O bond. The ultrasonic-assisted-microwave quick synthesis method and excellent NPCS support synergistically improved the catalytic activity and stability of Pd/NPCS catalyst. These findings provide insight into the design

* Corresponding authors at: College of Chemistry and Chemical Engineering, Guizhou University, Guiyang, Guizhou 550025, China.
E-mail addresses: linq@gzu.edu.cn (Q. Lin), hypan@gzu.edu.cn (H. Pan).

Peer review under responsibility of King Saud University. Production and hosting by Elsevier.



and preparation of efficient Pd catalysts for directly synthesizing H₂O₂ at atmospheric pressure.

© 2023 The Authors. Published by Elsevier B.V. on behalf of King Saud University. This is an open access article under the CC BY-NC-ND license (<http://creativecommons.org/licenses/by-nc-nd/4.0/>).

1. Introduction

Hydrogen peroxide (H₂O₂) exhibits both oxidizing and reducing properties. In chemical reactions, it acts as a reducing agent, producing only O₂ as a product, and as an oxidant, producing only H₂O as a product. It does not generate toxic by-products or substances that are challenging to separate and degrade, thus aligning with the principles of environmentally friendly practices and sustainable development. Its applications span various fields, including medicine, aerospace, and the electronics industry. Anthraquinone method is the primary method to synthesize H₂O₂ at present with some problems such as complicated process, high energy consumption and serious environmental pollution (Campos-Martin et al., 2006, Samanta 2008, Edwards et al., 2015, Ciriminna et al., 2016, Seo et al., 2016, Lewis and Hutchings 2018, Gao et al., 2020, Han et al., 2021). However, the direct synthesis of H₂O₂ from H₂ and O₂ with the advantages of green environmental protection, high atomic economy, and coupling with the reaction process that does not require high H₂O₂ concentration is expected to replace the anthraquinone method for H₂O₂ synthesis (Huang et al., 2016, Agarwal et al., 2017, Jin et al., 2020, Lewis et al., 2022). Compared with Pt, Au, Ag and other noble metal catalysts, Pd catalyst shows a better catalytic performance for H₂O₂ directly synthesizing (Samanta 2008, Rankin and Greeley 2012, Lewis and Hutchings 2018, Han et al., 2021). But it is worth noting that the reaction mechanism and reaction path for H₂O₂ directly synthesized from H₂ and O₂ over supported Pd catalysts indicate that the side reactions leading to water formation by unselective O₂ hydrogenation, H₂O₂ hydrogenation, and H₂O₂ decomposition caused by the breaking of O-O bonds are thermodynamically favorable compared to the main reaction that H₂O₂ directly synthesized from H₂ and O₂, which greatly affects the improvement of the catalytic performance for Pd catalyst. Consequently, reasonable design and simple synthesis of a highly efficient Pd catalyst has become the key issue to improving the catalytic performance for the direct synthesis of H₂O₂ from H₂ and O₂. At present, there have been many studies on the catalytic reaction mechanism, the morphology regulation, electronic structure and geometric structure regulation of Pd active component, the selection of catalyst supports, catalyst structure design, the preparation methods and optimization of reaction conditions and so on, aiming to weaken the excessive activation of O₂ by Pd catalyst which could lead to the breaking of O-O bonds, and inhibit the dissociation of species on the surface contained O-O bond, so as to improve the productivity and selectivity of H₂O₂ directly synthesized from H₂ and O₂ (Choudhary et al., 2006, Choudhary et al., 2006, Choudhary et al., 2007, Edwards et al., 2007, Liu et al., 2008, Staykov et al., 2008, Li et al., 2011, Li et al., 2011, Menegazzo et al., 2012, Abate et al., 2013, Freakley et al., 2013, Tian et al., 2013, Edwards et al., 2014, García-Serna et al., 2014, Han et al., 2017, Lari et al., 2017, Tian et al., 2017, Tian et al., 2019).

In the studies of Pd catalyst supports, carbon support has received close attention due to the advantages such as high specific surface area, rich pore structure, and tunable surface functionality (Edwards et al., 2008, Ntainjua N et al., 2008, Edwards et al., 2009, Abate et al., 2010, Piccinini et al., 2012, Arrigo et al., 2014, Hu et al., 2014, García et al., 2015, Arrigo et al., 2016, Yook et al., 2016, Lee et al., 2017, Lee et al., 2018, Ji et al., 2021, Lewis et al., 2021). Graham J. Hutchings team (Edwards et al., 2008, Ntainjua N et al., 2008) found that carbon support was the best support for Pd and AuPd catalysts because of the superior catalytic activity and lowest rate of H₂O₂ hydrogenation and decomposition side reactions. In the follow-up research works (Edwards et al., 2009, Piccinini et al., 2012, Lewis et al., 2021), the team further found that nitric acid pretreatment of

carbon supports for AuPd catalysts could switch off the sequential H₂O₂ hydrogenation and decomposition side reactions compared with TiO₂, ZrO₂, CeO₂ and other oxide supports, thereby achieving the target selectivity and producing a high rate of H₂O₂ synthesis under intrinsically safe conditions. Subsequent research (Hu et al., 2014, García et al., 2015, Yook et al., 2016, Lee et al., 2017, Lee et al., 2018) have also indicated that carbon support materials were effective supports for Pd catalyst, and H₂O₂ catalytic activity depended on the pore structure and surface properties of carbon supports. They found that the high specific surface area of carbon support facilitated dispersion of Pd active metal, which resulted in an increase of Pd metal surface area and Pd active sites. In addition, they believed that mesoporous carbon support was superior to microporous ones, and microporous carbon such as activated carbon suffered from diffusion limitation leading to significantly slower H₂ conversion than mesoporous catalysts. While previous research (Abate et al., 2010, Arrigo et al., 2014, Arrigo et al., 2016, Ji et al., 2021) have indicated that the introduction of nitrogen-doping for carbon support was not only a positive effect in dispersing Pd nanoparticles and stabilizing smaller Pd nanoparticles, but also an electronic effect on Pd nanoparticles. More electron-rich Pd nanoparticles would favor O₂ surface coverage and the rate for H₂O₂ synthesis. Therefore, it will be expected from the current research direction that carbon support has a good research and application prospect in the direct synthesis of H₂O₂ from H₂ and O₂. In particular, N-doped carbon support with high specific surface area and abundant pore structure not only facilitate the high dispersion of Pd active metals, but also improve the coverage of H₂ and O₂ reaction molecules on the surface of Pd catalyst at atmospheric pressure and increase the interaction between species on the surface containing O-O bonds (Tian et al., 2013), and enhance the mass transfer and diffusion performance of Pd catalysts, which improves the catalytic performance of Pd catalyst. However, the N-doped carbon support used in the current research work have low specific surface area, small pore volume and simple pore structure, while the N-doped carbon supports with high specific surface area and rich pore structure are less studied as the support of Pd catalyst.

In the studies of Pd catalyst preparation methods, the traditional preparation method of supported Pd catalyst is impregnation method, which has the characteristics of simple preparation process and high production capacity and is easy to large-scale industrial production. However, Pd active metal tend to aggregate to form large size Pd particles due to their high surface energy in the long-time and high-temperature heat treatment process, resulting in low catalyst activity. Therefore, quick synthesis and the avoidance of long-time high-temperature treatment for supported Pd catalyst could be beneficial to reduce time consumption and avoid agglomeration of Pd nanoparticles, realizing the uniform dispersion of Pd active sites, which is very necessary for the design of supported Pd catalyst and improving the catalytic performance. Pd catalyst supported on N-doped porous carbon support was quickly synthesized by using microwave and ultrasonic coupling technique with the rapid and selective heating characteristics of microwave, and the oscillation, dispersion, and cavitation of ultrasonic wave (Zhang et al., 2013, Ma et al., 2018, Wang et al., 2018, Zhou et al., 2018, Guo et al., 2022, Yuan et al., 2022) which can achieve controlling the Pd nanoparticles with a smaller particle size and a narrower particle size distribution range to improve the catalytic performance for H₂O₂ directly synthesizing. However, Pd catalyst supported on N-doped porous carbon support with high specific surface area and rich pore structure prepared by ultrasonic-assisted-microwave quick synthesis method has not been reported in H₂O₂ directly synthesized from H₂ and O₂ at atmospheric pressure.

Based on the current research works, mono-disperse, uniform-size and N-doped porous carbon sphere named as NPCS with high specific surface area and rich mixed micro-mesoporous pore structure was prepared by hydrothermal and one-step activation at high temperature using glucose as carbon source, PSSMA as a dispersant, potassium bicarbonate as an activator, melamine as nitrogen source and activator. Meanwhile, a series of Pd/NPCS catalysts were prepared by different catalyst synthesis methods which used in H_2O_2 directly synthesizing. Then, we focused on exploring the influence of ultrasonic-assisted-microwave synthesis condition on the catalytic performance for Pd/NPCS catalyst and screen out the optimal synthesis condition. Then, the optimal synthesis condition was selected to synthesize Pd/NPCS catalysts with different Pd loading and the influence of NPCS support properties and Pd loading on the catalytic performance for H_2O_2 directly synthesized from H_2 and O_2 at atmospheric pressure was researched in this study.

2. Experimental

2.1. Chemicals

Palladium chloride (PdCl_2 , 59–60 wt% of Pd), Poly (4-styrenesulfonic acid-co-maleic acid) sodium salt (PSSMA, the molar ratio of 4-styrene sulfonic acid to maleic acid was 1:1, Mw 19500-20500), Potassium bicarbonate (KHCO_3 , 99.5 wt%), Melamine ($\text{C}_3\text{H}_6\text{N}_6$, 99 wt%), and Ethylene glycol ($\text{C}_2\text{H}_6\text{O}_2$, 98 wt%) were purchased from Shanghai Aladdin Biochemical Technology Co., Ltd.; Glucose ($\text{C}_6\text{H}_{12}\text{O}_6$, 98 wt%) was purchased from Sinopharm Chemical Reagent Co., Ltd.; Ethanol ($\text{C}_2\text{H}_5\text{OH}$, 99.7 wt%) and Methanol (CH_3OH , 99.5 wt%) were purchased from Tianjin Fuyu Fine Chemical Co., Ltd. All reagents were used as received without further purification. Deionized water was used throughout the experiment process.

2.2. Preparation of the catalysts

As shown in Fig. 1, Pd/NPCS catalyst was prepared by ultrasonic-assisted-microwave quick synthesis method using mono-disperse, uniform-size and N-doped porous carbon sphere (NPCS) as the support and PdCl_2 as the palladium precursor. The specific synthesis steps are as follows.

2.2.1. Preparation of NPCS support

The hydrothermal carbon was prepared by the method mentioned in the literature (Xie et al., 2018). 6.0 g glucose and 70 mg PSSMA were dissolved in 50 ml deionized water to form a mixed solution which was continuously stirred at 25 °C for 2 h until the solution became clear. Then the solution was transferred to a 100 ml polytetrafluoroethylene-lined hydrothermal reaction kettle, and the hydrothermal reaction was performed in an oven at 180 °C for 8 h. After the hydrothermal reaction was completed, the reaction kettle was cooled to room temperature, and then the hydrothermal carbon was washed with deionized water and absolute ethanol until the filtrate was clear, and placed in an oven at 80 °C for drying. Next, the activation and N doping of the hydrothermal carbon were carried out by one-step activation at a high temperature currently being studied by our research group. Hydrothermal carbon, melamine, and potassium bicarbonate were mixed and fully ground according to the mass ratio of 1:2:8. After that, the mixture was loaded into a corundum porcelain boat and sent into a tube furnace, and pyrolyzed and activated in N_2 atmosphere. The temperature was raised to 400 °C at 5 °C/min for 2 h, and then to 900 °C at 5 °C/min for 1 h. The tube furnace was cooled to room temperature, and the black solid obtained was added into 150 ml 2 M

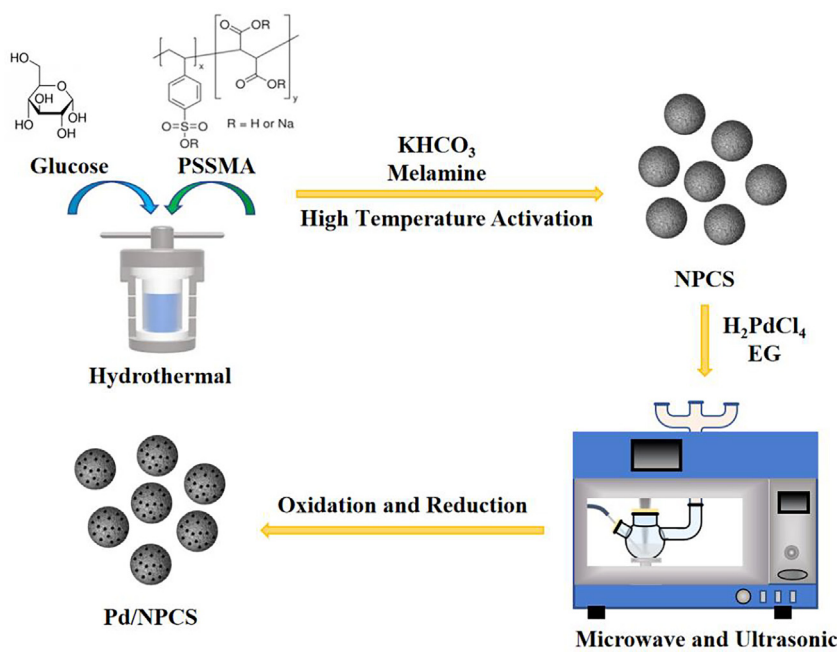


Fig. 1 Schematic diagram of Pd/NPCS catalyst prepared by ultrasonic-assisted-microwave quick synthesis method.

hydrochloric acid solution, and stirred at room temperature for 10 h. After washing with deionized water to neutral, the final N-doped porous carbon was dried overnight in an oven at 80 °C and denoted as NPCS.

2.2.2. Preparation of Pd/NPCS catalysts

A series of Pd/NPCS catalysts were prepared by impregnation method, wet chemical reduction method, deposition precipitation method, and ultrasonic-assisted-microwave quick synthesis method which named as Pd/NPCS(Y), and Y was the type of catalyst synthesis method.

Impregnation method: 0.1 g NPCS support was added into 50 ml deionized water and ultrasonic dispersed for 30 min to form a uniform dispersion. Then 0.5 ml 0.075 M H_2PdCl_4 solution was added drop by drop with a pipette gun, and the reaction was stirred continuously at 35 °C for 24 h. At the end of the reaction, the product was transferred to 80 °C oven and dried overnight, and the dried product was oxidized for 2 h under air and reduced for 2.5 h under H_2 atmosphere at 250 °C. The final prepared catalyst was denoted as Pd/NPCS(I).

Wet chemical reduction method: 0.1 g NPCS support was added into 50 ml deionized water and ultrasonic dispersed for 30 min to form a uniform dispersion. Then 0.5 ml 0.075 M H_2PdCl_4 solution was added drop by drop with a pipette gun, and the reaction was stirred continuously at 35 °C for 24 h. At the end of the reaction, 0.5 ml 5 wt% fresh NaBH_4 solution was added drop by drop and the reaction was continued at 35 °C for 3 h. The obtained reduced product was washed with deionized water and centrifuged for three times, and dried overnight in the oven at 80 °C, and the dried product was oxidized for 2 h under air and reduced for 2.5 h under H_2 atmosphere at 250 °C. The final prepared catalyst was denoted as Pd/NPCS(C).

Deposition precipitation method: 0.1 g NPCS support was added into 50 ml ethylene glycol and ultrasonic dispersed for 30 min to form a uniform dispersion, then 0.5 ml 0.075 M H_2PdCl_4 solution was added drop by drop, and the pH value was adjusted to about 10 with 1 M sodium hydroxide/glycol solution, and the reaction was continuously stirred at 160 °C for 6 h under reflux condition. The obtained reduced product was washed with ethanol and centrifuged for one time, then washed with deionized water and centrifuged for three times, and dried overnight in an oven at 80 °C. The dried product was oxidized for 2 h under air and reduced for 2.5 h under H_2 atmosphere at 250 °C. The final prepared catalyst was denoted as Pd/NPCS(D).

Ultrasonic-assisted-microwave quick synthesis method: Considering that too large ultrasonic intensity was not conducive to the loading of Pd active metal, and too small was not conducive to the dispersion of Pd active metal, so in the synthesis of Pd/NPCS(W) catalyst, the ultrasonic was turned on and kept at a low level. At the same time, the microwave power was kept at 750 W and the temperature programmed rate remained unchanged. Typical synthesis steps of Pd/NPCS catalyst prepared by ultrasonic-assisted-microwave quick synthesis method: 0.1 g NPCS support was added into 50 ml ethylene glycol and ultrasonic dispersed for 30 min to form a uniform dispersion. Then 0.3 ml 0.075 M H_2PdCl_4 solution was added drop by drop with a pipette gun, and the reaction was stirred continuously at 35 °C for 24 h. After stirring reaction, the reactant was ultrasonic dispersed for 5 min, and then

the pH value was adjusted to about 10 with 1 M sodium hydroxide/ethylene glycol solution. The reactant was rapidly reduced by Microwave-Ultrasonic-UV Synthesis (XH-300UL + Microwave-Ultrasonic-UV Synthesis, Beijing Xianghu Technology Limited Co., China). Microwave and ultrasonic parameters: microwave power was 750 W, and temperature programmed rate was from room temperature to 100 °C (3 min), 100-160°C (6 min), and 160 °C maintaining for 5 min; the ultrasonic intensity was low grade throughout the entire process. The obtained reduced product was washed with ethanol and centrifuged once, then washed with deionized water and centrifuged three times, and dried in an oven at 80 °C overnight. The dried product was oxidized for 2 h under air and reduced for 2.5 h under H_2 atmosphere at 250 °C. The final N-doped porous carbon in-situ supported Pd was denoted as Pd/NPCS(W) catalyst.

By changing the microwave reduction temperature (150 °C, 160 °C and 180 °C) and the microwave reduction time (5 min, 10 min, 15 min), we focused on exploring the influence of ultrasonic-assisted-microwave synthesis condition on the catalytic performance for Pd/NPCS catalyst and screen out the optimal synthesis condition. Then the Pd/NPCS catalysts with different Pd loading were synthesized under the optimal ultrasonic-assisted-microwave quick reduction condition, and the addition amounts of 0.075 M H_2PdCl_4 solution were 0.1 ml, 0.2 ml, 0.3 ml, 0.4 ml and 0.5 ml, respectively.

2.3. Characterization

Scanning electron microscopy (SEM, SIGMA, ZEISS, Germany) and transmission electron microscopy (TEM, Tecnai G2 F20, FEI, USA) were used to detect the microscopic morphology, structure and nanoparticle size of the samples. The phases of the samples were detected using an X-ray diffractometer (XRD, D8 Advance, Bruker, Germany). The elemental composition and chemical state on the surface of the samples were determined using an X-ray photoelectron spectrometer (XPS, K-Alpha Plus, Thermo Fisher Scientific, USA). Fourier transform infrared spectrometer (FT-IR, Nicolet is 50, Thermo Fisher Scientific, USA) was used to detect the functional group structure of the samples. The graphitization and defect degree of the samples were detected using a laser microscope confocal Raman spectrometer (LadRAM HR Evoluion, HORIBA, France). The elemental composition of N, C, and H of the samples was detected using an elemental analyzer (Elemental Analyser, Euro EA3000, EuroVector, Italy). The specific surface area and pore structure of the samples were determined using N_2 adsorption/desorption physical adsorption instrument (ASAP2460, Micrometrics, USA). The loading of Pd in the catalysts were determined using an inductively coupled plasma optical emission spectrometer (ICP-OES, iCAP 7200, Thermo Fisher Scientific, USA).

2.4. Catalytic activity test

The catalytic activity of Pd/NPCS(Y) catalysts for the direct synthesis of H_2O_2 from H_2 and O_2 were evaluated in a jacketed glass reactor at 0 °C and at atmospheric pressure. N_2 (99.999%) was used as the carrier gas, the reactants were H_2 (99.999%) and O_2 (99.995%), The total gas flow rate was 16.25 ml/min, including 2.25 ml/min for H_2 , 4 ml/min for

O₂, and 10 ml/min for N₂. A mixed solution with 160 ml methanol and 1.8 ml concentrated sulfuric acid were used as the reaction medium, and the mass of Pd/NPCS(Y) catalysts were about 10 mg. H₂O₂ concentration was measured through iodometric titration, and the content of H₂ and O₂ in the tail gas after the reaction were measured by GC-9860 gas chromatography.

The H₂ conversion, H₂O₂ selectivity, and H₂O₂ productivity were calculated using the following equations respectively:

$$H_2 \text{ conversion (\%)} = \frac{\text{moles of } H_2 \text{ reacted}}{\text{moles of } H_2 \text{ feed}} \times 100\%$$

$$H_2O_2 \text{ selectivity (\%)} = \frac{\text{moles of } H_2O_2 \text{ formed}}{\text{moles of } H_2 \text{ reacted}} \times 100\%$$

$$H_2O_2 \text{ productivity (mmol - } H_2O_2 / gPd \cdot h^{-1}) = \frac{\text{mmoles of } H_2O_2 \text{ formed}}{\text{weight of Pd(g) incatalyst} \times \text{reaction time(h)}}$$

The hydrogenation/decomposition experiments of Pd/NPCS(Y) catalysts were also evaluated in the above-mentioned jacketed glass reactor by the same reaction conditions, except that methanol solution containing 1 wt% H₂O₂ was introduced. The hydrogenation experiment was carried out in an atmosphere with a total flow rate of 12.25 ml/min containing 2.25 ml/min for H₂ and 10 ml/min for N₂, while the decomposition experiment only had a gas feed of pure N₂.

3. Results and discussion

The particle size and dispersion of Pd active metal will affect the catalyst activity. By selecting a suitable catalyst synthesis method, Pd nanoparticles could be evenly dispersed on the surface of carbon support with high specific surface area to reduce the possibility of agglomeration, which improve the catalytic activity of Pd catalyst. The XRD patterns of Pd/NPCS catalysts prepared by impregnation method, wet chemical reduction method, deposition precipitation method, and ultrasonic-assisted-microwave quick synthesis method are shown in Fig.S1, while the influence on catalytic performance for the direct synthesis of H₂O₂ from H₂ and O₂ at atmospheric pressure are shown in Fig. 2.

As can be seen from Fig.S1, both Pd/NPCS(I), Pd/NPCS(C) and Pd/NPCS(D) catalysts show the characteristic diffraction peaks of Pd(111), Pd(200), Pd(220), Pd(311) and Pd(222) crystal planes at 2θ value about of 40.0°, 46.5°, 67.8°, 81.7°, 86.2° respectively, which are in good agreement with the standard diffraction spectrum of Pd (JCPDS#87-0643), and indicating that the Pd nanoparticles in the catalyst all exist in the form of face-centered cubic structure(Tian et al., 2017). However for the Pd/NPCS(W) catalyst, only the characteristic diffraction peak of Pd(111) crystal plane can be observed, and the peak strength is weaker than that of Pd/NPCS(I), Pd/NPCS(C) and Pd/NPCS(D) catalysts, but the half-peak width is larger than that of the above catalysts. The mean particle sizes calculated by Scherrer's formula of Pd nanoparticles on Pd/NPCS(I), Pd/NPCS(C), Pd/NPCS(D) and Pd/NPCS(W) catalysts are 17.0 nm, 12.2 nm, 8.1 nm and 4.9 nm, respectively.

As can be seen from Fig. 2, Pd/NPCS(W) catalyst has the best catalytic activity for H₂O₂ directly synthesizing compared with Pd/NPCS(I), Pd/NPCS(C) and Pd/NPCS(D) catalysts.

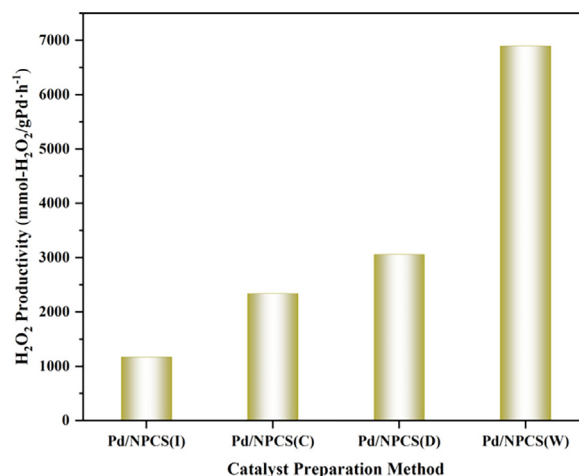


Fig. 2 The influence of preparation method on the catalytic performance for Pd/NPCS catalysts[*Reaction conditions: catalyst 10 mg, 160 ml MeOH, 1.8 ml 98 wt% H₂SO₄, total flow rate 16.25 ml/min, H₂:O₂:N₂ = 2.25:4:10, 120 rpm/min, 0 °C, atmospheric pressure, 1.0 h.].

Combined with the XRD characterization results in Fig.S1, it indicates that the preparation method of Pd catalyst will affect the dispersion and particle size of Pd active metal, further affecting the catalytic performance for H₂O₂ directly synthesizing from H₂ and O₂ at atmospheric pressure. Due to the poor interaction between Pd active metal and NPCCS support, Pd was easy to migrate and agglomerate to form large Pd nanoparticles during high-temperature reduction to the Pd/NPCS(I) catalyst synthesized by immersion method. While wet chemical reduction method also resulted in uneven dispersion of Pd active metal on the surface of NPCCS support due to solvation effect to the Pd/NPCS(C) catalyst. However, Pd/NPCS(D) catalyst prepared by deposition precipitation method can make some Pd nanoparticles larger because of long time and high-temperature reflux reduction. Compared with the above preparation methods, the ultrasonic-assisted-microwave quick synthesis method could not only significantly shorten the synthesis time of Pd catalyst by microwave and ultrasonic coupling technique with rapid and selective heating characteristics of microwave, and oscillation, dispersion, and cavitation of ultrasonic wave, but also enabled Pd nanoparticles to be uniformly dispersed on the NPCCS support, with a smaller particle size and a narrower particle size distribution range, which exposing more Pd active sites and improving H₂O₂ generation rate. Therefore, ultrasonic-assisted-microwave quick synthesis method was selected as the catalyst preparation method for the subsequent research work.

The addition amount of 0.075 M H₂PdCl₄ solution was kept at 0.5 ml, the ultrasonic intensity was at a low level, the microwave power was 750 W, and the programmed heating rate was unchanged, the evaluation results of microwave reduction temperature and microwave reduction time on the catalytic activity of Pd/NPCS(W) catalysts for the direct synthesis of H₂O₂ from H₂ and O₂ at atmospheric pressure are shown in Fig. 3, which are characterized by the H₂O₂ productivity measured at 1.0 h. As seen from the Fig. 3, microwave reduction temperature greatly influenced the catalytic activity of Pd/NPCS(W) catalysts. When the microwave reduction

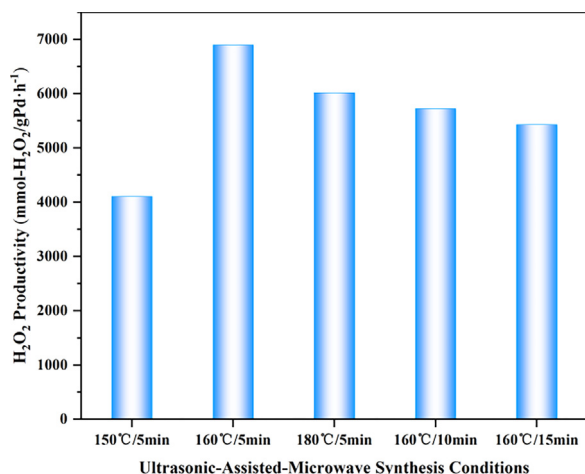


Fig. 3 The influence of ultrasonic-assisted-microwave synthesis conditions on the catalytic performance for Pd/NPCS(W) catalysts [*Reaction conditions: catalyst 10 mg, 160 ml MeOH, 1.8 ml 98 wt% H₂SO₄, total flow rate 16.25 ml/min, H₂:O₂:N₂ = 2.25:4:10, 120 rpm/min, 0 °C, atmospheric pressure, 1.0 h.].

temperature was 150 °C, the reduction ability of ethylene glycol was weak, which might lead to a large particle size of Pd nanoparticles and a small Pd⁰/Pd²⁺ ratio. Perhaps, there was still a small amount of Pd precursor PdCl₄²⁻ that had not been reduced in the solution which might be washed away during in the preparation process of Pd/NPCS(W) catalysts, resulting in lower catalytic activity. When the microwave reduction temperature was raised to 160 °C, Pd/NPCS(W) catalyst catalytic activity was the best and the H₂O₂ productivity was also the highest. When the microwave reduction temperature reached 180 °C, the reduction ability of ethylene glycol was greatly enhanced, however, higher reaction temperatures promote the aggregation of Pd nanoparticles on the surface of NPCS, ultimately leading to an increase in the particle size of Pd nanoparticles and a decrease in catalyst activity. XRD analysis (Fig.S5) of Pd/NPCS(W) catalysts prepared at different reduction temperatures provides strong evidence for this. The average particle sizes calculated by Scherrer's formula of Pd nanoparticles in Pd/NPCS(W) catalysts prepared at reduction temperatures of 150 °C, 160 °C, and 180 °C were calculated to be 5.8 nm, 5.1 nm, and 6.1 nm, respectively. At the same time, it could also be seen that the microwave reduction time had little effect on the catalytic activity of the Pd/NPCS(W) catalysts, but a longer microwave reduction time would affect the dispersion of Pd active metal. Therefore, the optimum microwave reduction temperature was 160 °C and the microwave reduction time was 5 min respectively. Then, the optimal synthesis condition was selected to synthesize Pd/NPCS(W) catalysts with different Pd loading. Following this, we focused on the effect of Pd loading and NPCS support property of Pd/NPCS(W) catalyst on the catalytic performance for the direct synthesis of H₂O₂ from H₂ and O₂ at atmospheric pressure in this research.

As can be seen from Fig. 4, the NPCS support obtained by high-temperature activation and N doping after PSSMA-assisted glucose hydrothermal treatment are mono-dispersed and uniform-size carbon nanospheres, which is consistent with the literature result(Xie et al., 2018). The average particle size of NPCS nanospheres is 427 nm, and the surface has an irreg-

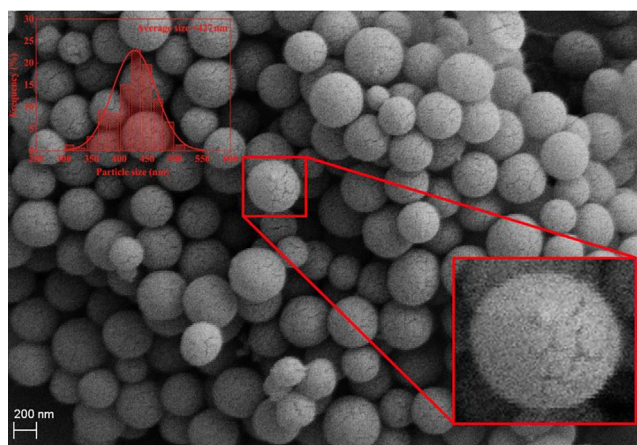


Fig. 4 SEM image and particle size distribution of NPCS support.

ular worm-like structure(Wang et al., 2019), which is conducive to the dispersion and attachment for Pd nanoparticles. As shown in Fig. 5(a1-e1 and a2-e2) Pd nanoparticles of Pd/NPCS(W) catalysts with different Pd loading are uniformly dispersed on the NPCS support, without an obvious agglomeration phenomenon. HRTEM images shown in Fig. 5(a3-e3) confirm the highly crystalline nature of Pd nanoparticles, and the d-spacings of adjacent fringe for Pd nanocrystals is about 0.23 nm, agreeing well with the Pd (111) lattice-spacing of face-centered cubic (fcc) Pd(Liu et al., 2008, Zhang et al., 2013, Ding et al., 2018). According to the histograms of Pd nanoparticle size (Fig. 5 a2-e2), it is evident that the average size of Pd nanoparticles increases with the progressive addition of H₂PdCl₄, which is likely attributed to the concentration of H₂PdCl₄ on the surface of NPCS support. As the amount of H₂PdCl₄ added increases, the concentration of H₂PdCl₄ in the ethylene glycol solution gradually rises, leading to enhanced adsorption of H₂PdCl₄ on the surface of NPCS support. During the high-temperature reduction process, the elevated H₂PdCl₄ concentration on the NPCS surface facilitates the formation of larger Pd nanoparticles. Notably, ultrasonic-assisted-microwave quick synthesis method, with its rapid heating and cavitation effects, results in a modest increase in the average particle size of Pd nanoparticles from 4.18 nm to 5.31 nm when the H₂PdCl₄ amount is raised from 0.1 ml to 0.5 ml. The particle size distribution diagram of Pd nanoparticles (Fig. 5 a2-e2) reveals that the particle size of Pd is primarily concentrated within the range of 2.0 nm to 7.5 nm. This observation indicates that the Pd nanoparticles synthesized using the ultrasound-assisted microwave method have a smaller and narrower particle size distribution overall. Additionally, they exhibit a higher degree of contact with active Pd sites, which greatly benefits the efficiency of direct H₂O₂ synthesis.

Fig. 6 shows that NPCS support has a broad diffraction peak at 2θ value of 23°, which corresponds to the (200) reflection of graphite, indicating that the carbon support is an amorphous structure. A relatively obvious diffraction peak appears at 2θ value of 43.6° can be assigned as the (100) reflection of graphite, indicating the partial graphitization of the carbon support(Deng et al., 2015, Shi et al., 2017, Zhang et al., 2020). And the strong baseline at the low angle region indicates

the successful formation of rich micro-mesopores in the carbon framework (Shi et al., 2017, Zhang et al., 2020). The same conclusion can also be drawn from the Raman spectra (Fig.S2), in which the D band at 1340 cm^{-1} represents the lattice defect of the C atom, while the G band at 1587 cm^{-1} demonstrates the in-plane vibration of the sp^2 carbon atoms. Typically, the intensity ratio between the D and G bands (I_D/I_G) is an index to evaluate the defect degree in the carbon materials (Deng et al., 2015, Shi et al., 2017, Zhu et al., 2018, Pu et al., 2020). The I_D/I_G intensity ratio of the NPCS support is 1.09, which confirmed that high temperature activation and N doping promoted the generation of defects in NPCS support.

Pd/NPCS(W) catalysts with different loading all show the characteristic diffraction peak of the Pd(111) crystal plane at 2θ value of 40.0° (Zhang et al., 2013, Chen et al., 2017, Tian et al., 2017, Liu et al., 2019), and all the catalysts have similar face-centered cubic (fcc) crystal structure, which are in good agreement with the standard diffraction spectrum of Pd (JCPDS#87-0643). The characteristic diffraction peaks of Pd (111) crystal planes are gradually obvious with the increase of Pd loading, but the characteristic diffraction peaks of Pd (200), Pd(220), Pd(311) and Pd(222) crystal planes are not obvious at 2θ value of 46.5° , 67.8° , 81.7° and 86.2° . Meanwhile, it can be seen that the characteristic peak at 2θ value of 43.6° of NPCS support becomes less obvious with the increase of Pd loading.

The results of XPS analysis and elemental analysis (Table S1) show that NPCS support is mainly composed of

C element. The N content measured by elemental analysis is about 1.18 wt%, which is higher than that of XPS analysis. Because elemental analysis characterizes the N element content of the NPCS support while XPS analysis is a surface analysis technology. Due to the low content of N element, the characteristic peak of N in the XPS survey of NPCS support (Fig. S3 (a)) is not obvious. In order to better study the chemical state of elements on the surface of NPCS support, high-resolution XPS was performed for the C1s, O1s, and N1s core level region. According to the C1s high-resolution spectrum (Fig. S3(b)), the characteristic peak of binding energy at 284.8 eV is assigned to the aromatic carbon C-C, the characteristic peak of 286.2 eV is assigned to C-O, and the characteristic peak of 288.7 eV is assigned to O-C = O, and a satellite peak corresponding to the $\pi-\pi^*$ transition is detected near 290.9 eV, which corresponds to the existence of graphene nanoplatelet microstructure (Shi et al., 2017, Cai et al., 2020, Mao et al., 2020, Zhang et al., 2020), this is consistent with the XRD results. The O1s high-resolution spectrum (Fig. S3 (c)) can be deconvoluted into three peaks, which correspond to C = O (531.7 eV), C-O (533.4 eV), and O-C = O (534.9 eV) respectively (Shi et al., 2017, Cai et al., 2020). The high-resolution spectrum of N1s (Fig. S3(d)) could be resolved into four types of N species with the domination of pyridinic-N, pyrrolic-N, graphitic-N and pyridine N-oxide at 398.37 eV, 400.1 eV, 401.6 eV and 403.7 eV, respectively (Zhu et al., 2018, Mao et al., 2019, Cai et al., 2020, Jia et al., 2020, Zhang et al., 2020, Wu et al., 2021). The graphitic nitrogen is the main nitro-

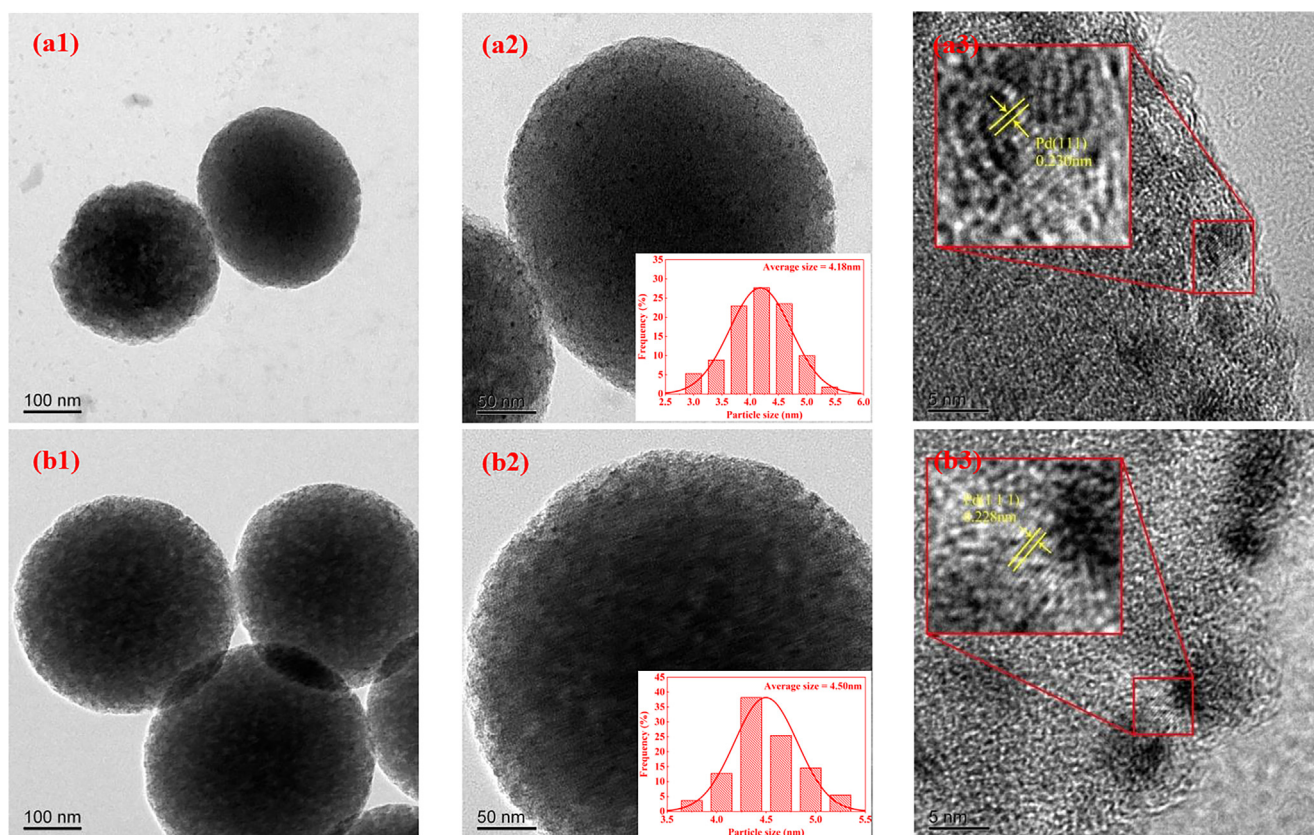


Fig. 5 (a1-a3), (b1-b3), (c1-c3), (d1-d3) and (e1-e3) TEM images of Pd/NPCS(W) catalysts with different loading at different magnifications and HRTEM images of Pd nanoparticles and the insets indicate the histograms of Pd nanoparticle size.

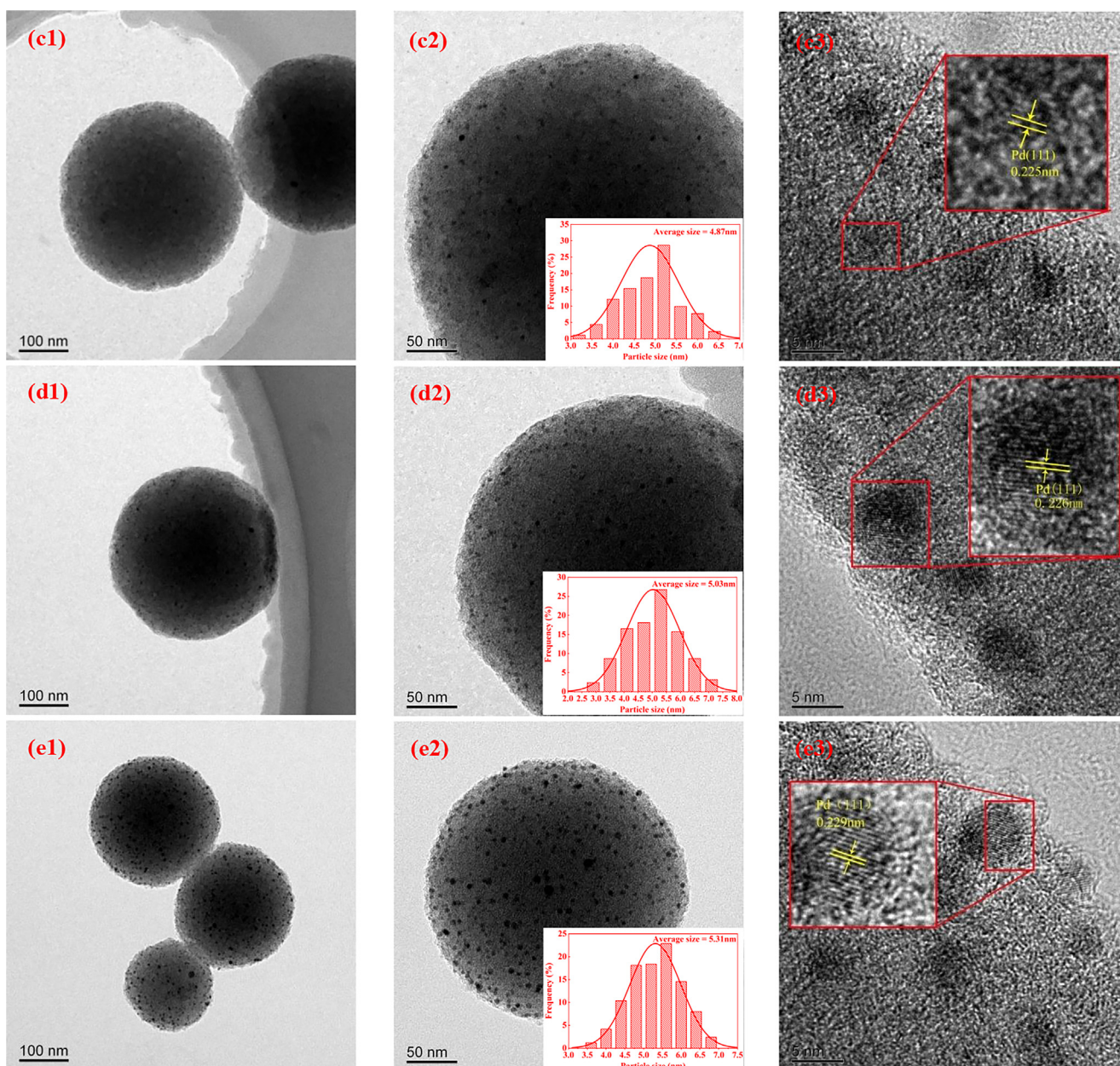


Fig. 5 (continued)

gen blending type which indicating that in the high-temperature activation process, N radicals generated by melamine pyrolysis were successfully doped into the aromatic carbon skeleton of the carbon support, forming stable N-containing functional groups. According to the research results of Rosa Arrigo and Salvatore Abate, as well as our research group (Arrigo et al., 2014, Arrigo et al., 2016), (Jiang et al., 2023), the nitrogen doping of NPCS support could regulate the electronic structure of carbon support and produce localized charge accumulation on the carbon surface which act as coordinative site for small Pd nanoparticles, but also an electronic effect on Pd nanoparticles that would favor O_2 surface coverage and the rate of H_2O_2 synthesis. At the same time, the FT-IR spectra of the NPCS support (Fig.S4) also present that a strong peak at 3443 cm^{-1} was caused by asymmetry

stretching vibration of the N-H and O-H bonds (Cai et al., 2020, Cuong et al., 2020). The weaker peak at 2920 cm^{-1} and 2849 cm^{-1} are correlated with the stretching vibration of aliphatic hydrocarbon $-CH_3$ and $-CH_2$ groups (Xie et al., 2018, Cai et al., 2020, Cuong et al., 2020). Furthermore, the weaker peak at 1384 cm^{-1} can be assigned to the stretching vibration of $-CH_3$ group (Cai et al., 2020), and the characteristic peaks near 1578 cm^{-1} and 1202 cm^{-1} can be attributed to the vibrational stretching of N-O and C = C bonds (Cai et al., 2020, Chang et al., 2020, Cuong et al., 2020).

In particular, as shown in Fig. 7, the detailed parameters of Pd3d spectra for Pd/NPCS(W) catalysts with different loading suggest that Pd mainly exists in the form of metallic state (Pd^0) and oxidized state (Pd^{2+}) with two pairs of characteristic peaks which the peaks near 335.60 eV and 340.86 eV can be

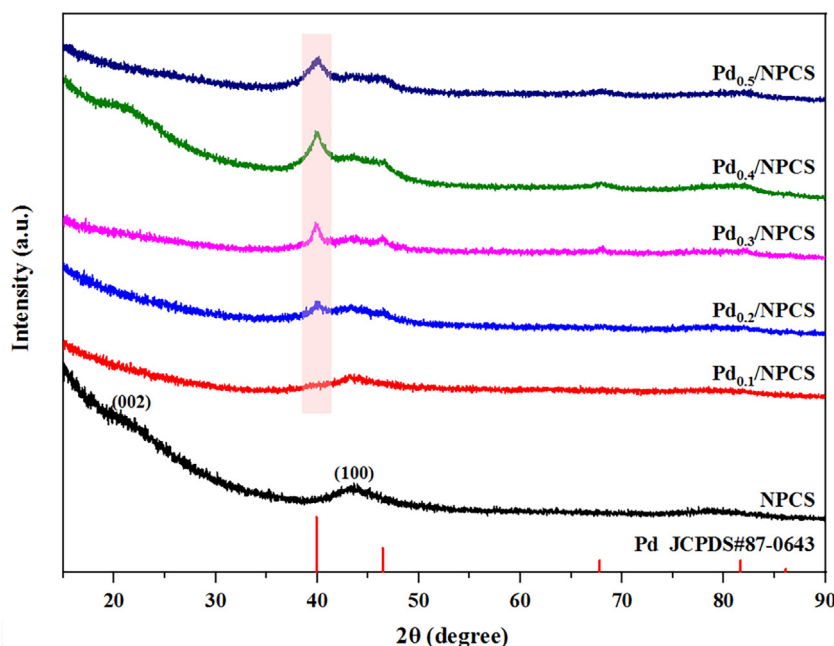


Fig. 6 XRD patterns of NPCS support and Pd/NPCS(W) catalysts with different Pd loading.

assigned to Pd^0 $3d_{5/2}$ and Pd^0 $3d_{3/2}$, while the peaks near 336.80 eV and 341.98 eV can be attributed to Pd^{2+} $3d_{5/2}$ and Pd^{2+} $3d_{3/2}$ (Tian et al., 2017, Ji et al., 2021, Lewis et al., 2021). Therefore, both Pd^0 and Pd^{2+} species are present in Pd nanoparticles of Pd/NPCS(W) catalysts treated by ultrasonic-assisted-microwave quick reduction and redox treatment. The relative content of each Pd species in the catalyst are listed in Table 1, the ratio of $\text{Pd}^0/\text{Pd}^{2+}$ increases from 0.82 in $\text{Pd}_{0.1}/\text{NPCS}(\text{W})$ to 1.71 in $\text{Pd}_{0.5}/\text{NPCS}(\text{W})$ with the increase of Pd loading. Previous studies (Tian et al., 2017, Ji et al., 2021, Lewis et al., 2021) have suggested that the chemical state of Pd nanoparticles affected the catalytic behavior. Pd^0 is the main active site for catalytic H_2 dissociation, while the presence of Pd^{2+} can inhibit H_2O_2 decomposition and increase H_2O_2 selectivity. Consequently, a certain proportion of $\text{Pd}^0/\text{Pd}^{2+}$ composition can not only promote H_2 dissociation activation to improve H_2 conversion rate and H_2O_2 productivity, but also provide non-dissociation activation active sites of O_2 to avoid excessive activation that resulted in O-O bond breaking and the dissociation of surface species containing O-O bond, which is conducive to improving H_2O_2 productivity and H_2O_2 selectivity.

It can be seen from Fig. 8(a) that the N_2 adsorption/desorption isotherm of NPCS support belongs to the typical type IV isotherm according to the IUPAC classification (Gong et al., 2014, García et al., 2015, Zhang et al., 2021). At lower relative pressure ($P/P_0 < 0.01$), N_2 adsorption capacity increases sharply with the increase of relative pressure, indicating that there is a large number of microporous pore structure in the carbon support. At higher relative pressure ($P/P_0 = 0.50-0.98$), the adsorption and desorption curve show an H2-type hysteresis loop due to capillary condensation in the mesopores. At the same time, the DFT pore size distribution diagram in Fig. 8 (b) further indicates that the NPCS support has a large number of micropores with pore size ranging from 0.5 nm to 1.5 nm and mesopores with pore sizes ranging from 2 nm to 5 nm,

which features the hierarchical nature of dominant micropores and small mesopores, consistent with the XRD results. Previous research has indicated that porous media exhibit robust mass transfer and diffusion capabilities (Zhao et al., 2023). Table 2 shows that the specific surface area of NPCS support is up to $3410.6 \text{ m}^2/\text{g}$, the total pore volume is $2.33 \text{ cm}^3/\text{g}$, the micropore volume is $0.63 \text{ cm}^3/\text{g}$, and the mesoporous ratio is 72.96 %. This indicates that in the high-temperature activation process, a large amount of potassium bicarbonate first decomposed to generate H_2O , CO_2 and other small gas molecules to etch the hydrothermal carbon, making the surface of hydrothermal carbon initially form microporous pore structure. After that, melamine decomposed at high temperature and produced a large amount of volatile gas, which further etched the hydrothermal carbon surface and promoted the formation of mesopores on the carbon surface. At the constant temperature stage of $900 \text{ }^\circ\text{C}$, molten potassium carbonate gradually penetrated into the interior of carbon through abundant pores on the surface of hydrothermal carbon, further promoting the formation of internal pores (Cuong et al., 2021). At the same time, N-radicals generated by melamine pyrolysis were successfully doped into the aromatic carbon skeleton of the carbon support. N-doped, high specific surface area and abundant mixed micro-mesoporous pore structure were not only conducive to guarantee good dispersion and anchoring of Pd nanoparticles, but also beneficial to the adsorption of reactants H_2 and O_2 to improve the coverage of H_2 and O_2 reaction molecules on the surface of Pd catalyst at atmospheric pressure, and increase the interaction between surface species containing O-O bonds to better react at the Pd active sites to generate H_2O_2 (Tian et al., 2013, Chen et al., 2021), then the H_2O_2 could be desorbed from the Pd active sites in time to the reaction solution, which enhances the transfer and diffusion performance for the Pd/NPCS(W) catalysts and effectively inhibiting the hydrogenation and decomposition side

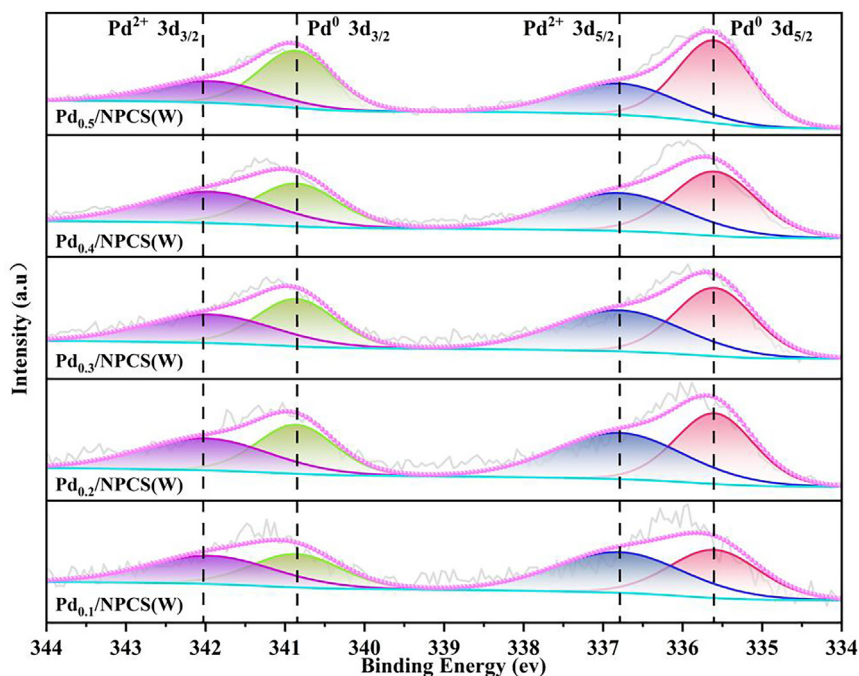


Fig. 7 Pd3d spectra of Pd/NPCS(W) catalysts with different Pd loading.

Table 1 Pd3d XPS spectra quantitative analysis of Pd/NPCS(W) catalysts with different Pd loading.

Catalysts	Pd3d _{3/2} (eV)		Pd3d _{5/2} (eV)		Pd ⁰ (%)	Pd ²⁺ (%)	Pd ⁰ /Pd ²⁺
	Pd ⁰	Pd ²⁺	Pd ⁰	Pd ²⁺			
Pd _{0.1} /NPCS(W)	340.86	341.98	335.60	336.80	45.03	54.97	0.82
Pd _{0.2} /NPCS(W)	340.86	341.98	335.60	336.80	47.83	52.17	0.92
Pd _{0.3} /NPCS(W)	340.86	341.98	335.60	336.80	50.60	49.40	1.02
Pd _{0.4} /NPCS(W)	340.86	341.98	335.60	336.80	55.19	44.81	1.23
Pd _{0.5} /NPCS(W)	340.86	341.98	335.60	336.80	63.04	36.96	1.71

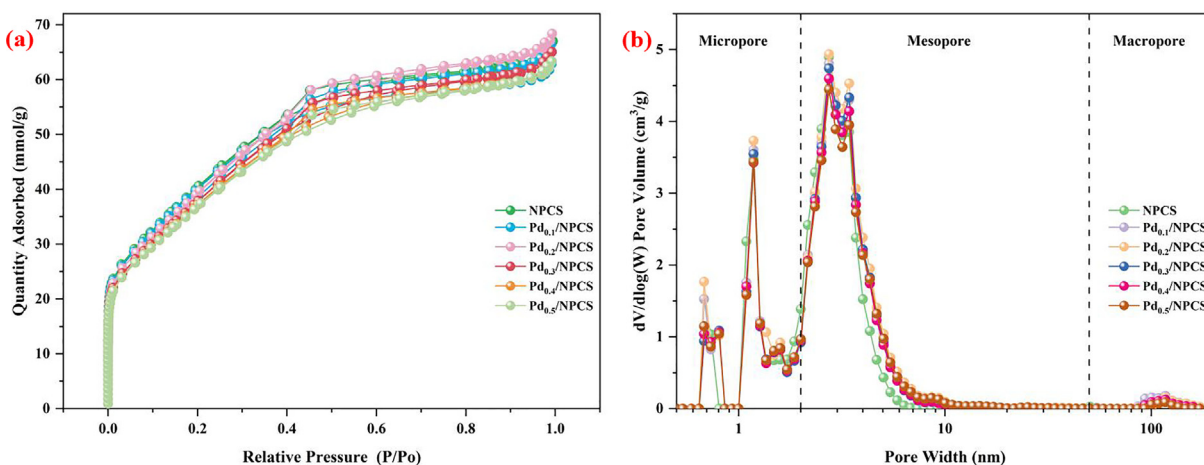


Fig. 8 (a) N₂ adsorption/desorption isotherm of NPCS support and Pd/NPCS(W) catalysts with different Pd loading (b) Pore size distribution of NPCS support and Pd/NPCS(W) catalysts with different Pd loading [The pore size distribution of NPCS support and Pd/NPCS(W) catalysts with different Pd loading calculated by density function theory (DFT)].

Table 2 Textural properties derived from the N₂ adsorption/desorption isotherm of NPCS support and Pd/NPCS(W) catalysts with different Pd loading.

Samples	S _{BET} (m ² /g) ^a	V _{Total} (cm ³ /g) ^b	V _{Mic} (cm ³ /g) ^c	V _{Mic} /V _{Total} (%)
NPCS	3410.6	2.33	0.63	27.04
Pd _{0.1} /NPCS(W)	3280.6	2.31	0.54	23.38
Pd _{0.2} /NPCS(W)	3256.7	2.28	0.53	23.25
Pd _{0.3} /NPCS(W)	3219.2	2.26	0.52	23.01
Pd _{0.4} /NPCS(W)	3158.2	2.22	0.51	22.97
Pd _{0.5} /NPCS(W)	3124.0	2.20	0.50	22.73

^a Specific surface area of NPCS support and Pd/NPCS(W) catalysts with different Pd loading calculated by Brunauer-Emmert-Teller (BET) method.

^b The total pore volume of NPCS support and Pd/NPCS(W) catalysts with different Pd loading calculated from the adsorption amount at P/P₀ = 0.995.

^c Micropore volume of NPCS support and Pd/NPCS(W) catalysts with different Pd loading calculated by t-Plot model.

reactions caused by the breaking of the O-O bond, thereby improving H₂O₂ selectivity.

In particular, the N₂ adsorption/desorption isotherm and DFT pore size distribution of Pd/NPCS(W) catalysts with different loading are similar to those of NPCS support, indicating that NPCS support is an excellent support for Pd catalysts. At the same time, as can be seen from Table 2 that with the increase of Pd loading, although the specific surface area, total pore volume, and micropore volume of the Pd/NPCS(W) catalysts all decrease slightly, which may be caused by Pd nanoparticles occupying part of the pores. However, the Pd/NPCS(W) catalysts with different loading still have good transfer and diffusion property, and the catalytic performance and stability of Pd/NPCS(W) catalysts can be improved.

Fig. 9 shows the catalytic performance evaluation of Pd/NPCS(W) catalysts with different loading for the direct synthesis of H₂O₂ from H₂ and O₂ at atmospheric pressure, and the H₂O₂ productivity, H₂ conversion and H₂O₂ selectivity were measured at 1.0 h. Fig. 8 illustrates an increasing conversion rate of H₂ with the increment of Pd loading, contrasting the decreasing selectivity of H₂O₂ and the volcano-shaped distribution of its productivity. Previous research has indicated that the crystal surface composition (Tian et al., 2013), the particle size (Tian et al., 2017), and the Pd⁰/Pd²⁺ ratio (Ao et al., 2016, Zhang et al., 2021) of Pd nanoparticles have a significant impact on the catalytic performance of the direct synthesis of H₂O. XRD (Fig. 6) and TEM (Fig. 5) analysis have shown that Pd nanoparticles in the Pd/NPCS(W) catalyst prepared by a microwave-assisted and ultrasound-assisted combined

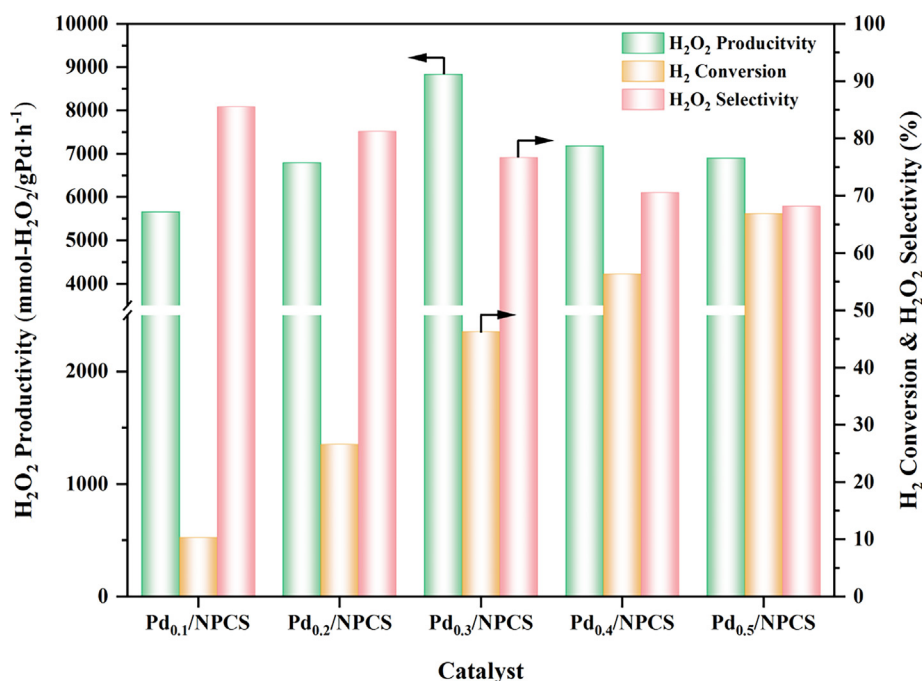


Fig. 9 Catalytic performance evaluation of Pd/NPCS(W) catalysts with different Pd loading for the direct synthesis of hydrogen peroxide from hydrogen and oxygen [*Reaction conditions: catalyst 10 mg, 160 ml MeOH, 1.8 ml 98 wt% H₂SO₄, total flow rate 16.25 ml/min, H₂:O₂:N₂ = 2.25:4:10, 120 rpm/min, 0 °C, atmospheric pressure, 1.0 h.].

rapid reduction are primarily dominated by Pd (111) crystal surface, with an average particle size ranging from 4.18 nm to 5.31 nm. Thus, it can be inferred that the crystal surface and particle size are not the main factors affecting the catalytic performance of Pd/NPCS(W) catalysts. When Pd loading was low, Pd nanoparticles provided fewer active sites, and the Pd3d XPS spectra analysis results also showed that the Pd⁰/Pd²⁺ ratio was relatively low at the same time, which had weak adsorption and dissociation activation of H₂ molecular and resulted in low H₂ conversion and H₂O₂ productivity. However, the lower loading of Pd active component also meant that there were fewer high-energy active sites (edges, corners) (Tian et al., 2017) on the Pd nanoparticles, and more Pd²⁺ species made the Pd nanoparticles have more positive charges, which moderate the bonding strength of O₂ molecule on the Pd active sites, and promote non-dissociative activation of O₂ molecule, thereby improving the H₂O₂ selectivity. Then, the increased Pd active sites promoted efficient H₂ conversion and H₂O₂ productivity, but decreased the H₂O₂ selectivity with Pd loading appropriate increasing. When Pd loading was continued to increase, the Pd⁰/Pd²⁺ ratio also increased with Pd loading, which meant that the continuous Pd⁰ sites on the Pd nanoparticles obviously increased to enhance adsorption and dissociation activation of H₂ molecular and improved H₂ conversion rate. However, more continuous Pd⁰ sites were also very active for the dissociation activation of O₂ molecule, resulting in the breaking of the O-O bond and aggravating the side reaction of hydrogenation and decomposition to generate H₂O, which decreased in both H₂O₂ productivity and H₂O₂ selectivity which were consistent with literature research results (Tian et al., 2013, Tian et al., 2017).

Interestingly, compared with Pd/NPCS(I), Pd/NPCS(C), and Pd/NPCS(D) catalysts, Pd/NPCS(W) catalysts with different loadings exhibit excellent catalytic activity for H₂O₂. This fully demonstrates that the ultrasonic-assisted microwave quick synthesis method is an effective strategy for synthesizing Pd catalysts. The method utilizes microwave heating for rapid and efficient selective heating, significantly reducing the high-temperature treatment time of Pd catalysts. Additionally, the oscillation, dispersion, and cavitation effects of ultrasound improve the dispersion of Pd active metal. The Pd/NPCS(W) catalyst prepared by the ultrasonic-assisted microwave quick synthesis method has the characteristics of uniform Pd nanoparticle loading, small particle size, narrow size distribution range, and insignificant increase in particle size with increasing loading. The crystal surface structure of Pd nanoparticles is primarily composed of the Pd(111) plane, which is the dominant plane for H₂O₂ generation (Tian et al., 2013). The Pd(111) plane enhances the adsorption and dissociative activation of H₂ molecules while ensuring the adsorption and non-dissociative activation of O₂ molecules, thereby facilitating the production of H₂O₂. Meanwhile, the introduction of nitrogen doping into the framework of NPCS support could make the Pd nanoparticles adhere more firmly on the carbon support, which further improved the stability of the Pd/NPCS(W) catalysts. More importantly, the NPCS support with a high specific surface area and abundant mixed mesoporous pore structure was conducive to the adsorption of reactants H₂ and O₂ to react with Pd active sites and the generated H₂O₂ could be desorbed from the Pd active sites in time to the reaction solution, which enhanced the transfer and diffusion performance for the Pd/NPCS(W) catalysts

and effectively inhibited the hydrogenation and decomposition side reactions caused by the breaking of the O-O bond at the same time, thereby improving H₂O₂ selectivity. Both ultrasonic-assisted-microwave quick synthesis method and the excellent NPCS support synergistically improved catalytic activity and stability of Pd/NPCS(W) catalysts.

Fig. 9 also shows that the catalytic performance of Pd_{0.3}/NPCS(W) catalyst was better when the addition amount of 0.075 M H₂PdCl₄ solution was 0.3 ml. The long-term activity evaluation experiment, hydrogenation and decomposition experiment of Pd_{0.3}/NPCS(W) catalyst were conducted for 3 h, and the evaluation results are shown in Fig. 10 and Fig. 11, respectively. As shown in Fig. 10, the catalytic performance of Pd_{0.3}/NPCS(W) catalyst was characterized by the H₂O₂ productivity, H₂ conversion and H₂O₂ selectivity measured at 0.5 h interval within 3 h. In the first 0.5 h, the catalytic activity of Pd_{0.3}/NPCS catalyst was higher. The Pd loading of Pd_{0.3}/NPCS catalyst was measured by ICP-OES to be about 2.5 wt%, the appropriate Pd loading provided sufficient active sites with Pd⁰/Pd²⁺ ratio was 1.39 and the amount of Pd⁰ was a little higher than that of Pd²⁺. Those meant a strong adsorption and dissociation activation of H₂ molecule, and moderated the bonding strength of O₂ molecule to promote non-dissociation activation of O₂ molecule, which was very important for H₂O₂ productivity and H₂O₂ selectivity at atmospheric pressure. In addition, it should also be considered that H₂O₂ concentration in the reaction system was low at the initial stage which was conducive to the forward reaction. After 0.5 h, with the extension of reaction time, H₂O₂ productivity, H₂ conversion and H₂O₂ selectivity decreased significantly, but the decreased amplitude became slow. On the one hand, the increase of H₂O₂ concentration in the reaction system inhibited the forward reaction. On the other hand, part of Pd⁰ sites on Pd nanoparticles were oxidized to Pd²⁺ under the harsh reaction conditions with H₂ conversion rate reducing. However, the appropriate amount of Pd active sites, Pd⁰/Pd²⁺ ratio and N-containing functional groups on NPCS support were beneficial to the resistance of Pd_{0.3}/NPCS(W) catalyst to the harsh reaction process (Arrigo et al., 2014, Arrigo et al., 2016). Moreover, the good transfer and diffusion performance of NPCS support enabled the generated H₂O₂ to disperse from Pd active sites into the reaction solution in time, which effectively inhibited the hydrogenation and decomposition side reactions caused by the breaking of the O-O bond, and further improved H₂O₂ productivity and H₂O₂ selectivity. Therefore, the deactivation rate of the Pd_{0.3}/NPCS(W) catalyst became slower after 0.5 h.

The stability of catalysts is an important characteristic. We analyzed the content, geometric, and electronic structure of Pd_{0.3}/NPCS(W) after a reaction time of 3 h using ICP-OES, XRD, and XPS. The Pd loading amount after the reaction was determined to be 2.48 wt% (Table S2), indicating negligible leaching of Pd during the reaction process. XPS analysis (Fig.S6) showed that the surface Pd⁰ of Pd_{0.3}/NPCS(W) only decreased by 0.45 % before the reaction, indicating good oxidation resistance of Pd_{0.3}/NPCS(W). XRD analysis revealed a change in the crystal plane composition of Pd_{0.3}/NPCS(W) during the reaction, with the emergence of crystal planes such as (100) that are unfavorable for H₂O₂ production (Fig.S7). The average particle size of Pd, calculated using the Scherrer formula, was determined to be 13.2 nm, suggesting agglomeration of Pd during the catalytic reaction process.

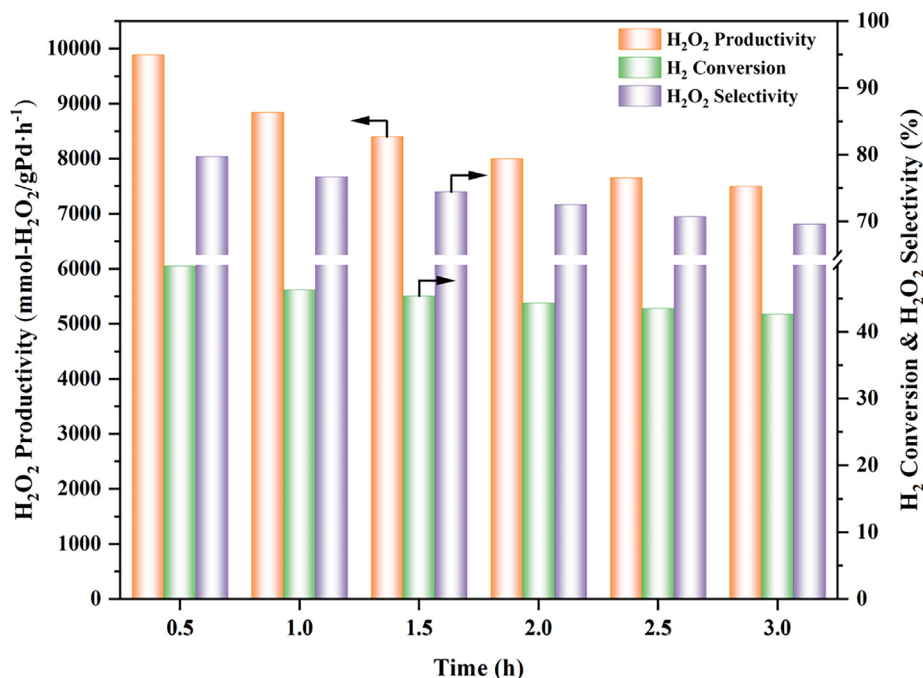


Fig. 10 Catalytic performance evaluation of Pd_{0.3}/NPCS(W) catalyst [*Reaction conditions: catalyst 10 mg, 160 ml MeOH, 1.8 ml 98 wt % H₂SO₄, total flow rate 16.25 ml/min, H₂:O₂:N₂ = 2.25:4:10, 120 rpm/min, 0 °C, atmospheric pressure, 3.0 h.].

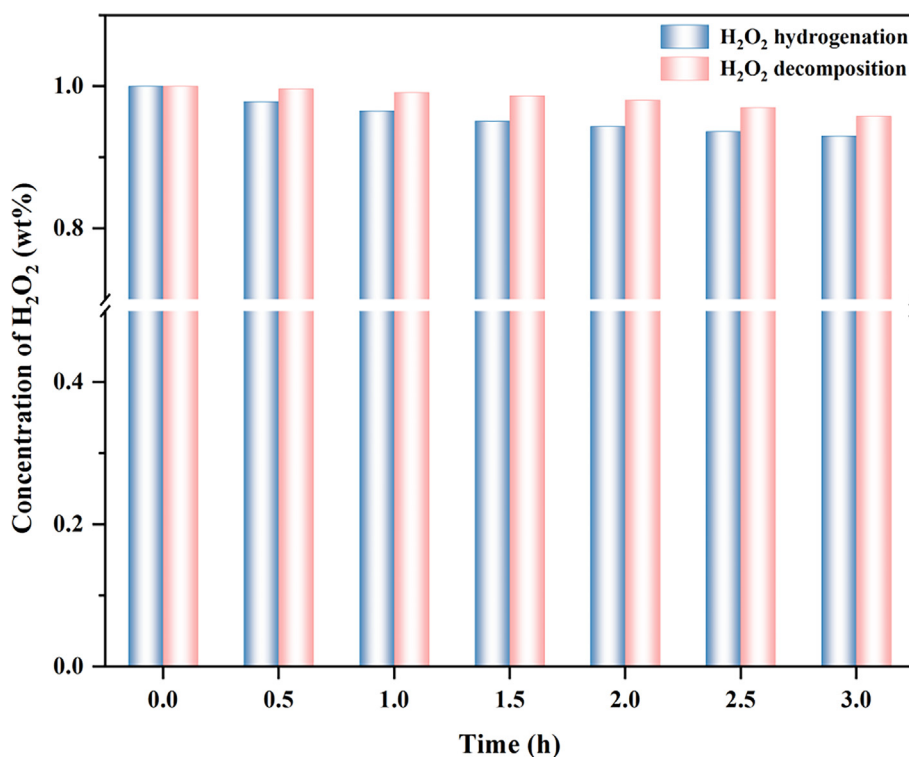


Fig. 11 H₂O₂ hydrogenation and decomposition evaluation of Pd_{0.3}/NPCS(W) catalyst [*Reaction conditions: catalyst 10 mg, 160 ml MeOH, 1.8 ml 98 wt% H₂SO₄, H₂O₂ initial concentration 1 wt%, total flow rate 12.25 ml/min, H₂:O₂:N₂ = 2.25:0:10 for H₂O₂ hydrogenation or total flow rate 10 ml/min, H₂:O₂:N₂ = 0:0:10 for H₂O₂ decomposition, 120 rpm/min, 0 °C, atmospheric pressure, 3.0 h.].

Fig. 11 shows that the degree of hydrogenation side reaction of Pd_{0.3}/NPCS(W) catalyst is greater than that of decomposition side reaction, which is consistent with the reported

research results of Pd catalysts (Thuy Vu et al., 2020). It indicated that Pd nanoparticles with smaller particle size provided more active sites for H₂ and O₂ adsorption and reacted with Pd

Table 3 Comparison of the catalytic activity of Pd_{0.3}/NPCS(W) with reported Pd catalysts supported on various carbon materials.

Catalysts	Pd loading /wt%	H ₂ O ₂ selectivity /%	H ₂ O ₂ Productivity /mol-H ₂ O ₂ /kg _{cat} ·h ⁻¹	Surface area /m ² /g	Pore volume /cm ³ /g	Preparation method ^c	Ref.
Pd _{0.3} /NPCS ^{a1}	2.5	76.7	219 ^b	3410.6	2.33	W	This work
Pd/NPCS(D) ^{a1}	4.1	–	125 ^b	3410.6	2.33	D	This work
Pd/S-ACR ^{a2}	2	87	42 ^b	886.2	0.8	I	(Thuy Vu et al., 2020)
Pd/XC-72 ^{a3}	2.5	74	129	227	0.56	C	(Hu et al., 2014)
Pd/PCs ^{a1}	4.6	66.7	228	1770	0.99	C	(Jiang et al., 2023)
Pd/NPCs ^{a1}	3.8	60.5	256	3421	2.16	C	(Jiang et al., 2023)

^{a1} Reaction conditions: catalyst (10 mg), 160 ml MeOH, 1.8 ml 98 wt% H₂SO₄, total flow rate 16.25 ml/min at atmospheric pressure, H₂:O₂:N₂ = 2.25:4:10, 100 rpm/min, 0 °C, 1 h.

^{a2} Reaction conditions: Catalyst (20 mg), 50 g MeOH/water (80 wt MeOH), total flow rate 16.25 ml/min, H₂: O₂: N₂ = 3.8:5.0:91.2, 1200 rpm, 275 K, 30 bar, 1 h.

^{a3} Reaction conditions: catalyst (50 mg), 50 ml EtOH and 10 ml water, HCl concentration 28 mmol/l, total gas flow rate of 60 ml/min (H₂:O₂:N₂ = 1:4:1) at atmospheric pressure, 10 °C, and 4 h.

^b The value of productivity was converted to mol-H₂O₂/kg_{cat}·h⁻¹ for a convenient comparison of this work with literature data.

active sites at atmospheric pressure, but that also increased the surface unsaturated sites which caused the breaking of O-O bonds and aggravates the side reaction of hydrogenation and decomposition to generate H₂O. However, it was worth noting that in the hydrogenation and decomposition experiments, the H₂O₂ concentration in the reaction solution decreased slowly and remained above 90 % after the reaction for 3 h, indicating that the high specific surface area and abundant mixed micro-mesoporous pore structure of NPCS support were conducive to enhance the transfer and diffusion performance for Pd_{0.3}/NPCS(W) catalyst. So that the generated H₂O₂ could be desorbed from the Pd active sites in time to the reaction solution, and effectively inhibited the hydrogenation and decomposition side reactions caused by the breaking of the O-O bond. At the same time, adding an appropriate amount of concentrated sulfuric acid as an acid stabilizer to the reaction system could inhibit the decomposition of H₂O₂ and improve H₂O₂ selectivity, which were consistent with the evaluation results of catalytic performance.

The catalytic performance of Pd_{0.3}/NPCS catalyst with other carbon-supported Pd catalysts is compared in Table 3. As shown in Table 3, Pd_{0.3}/NPCS catalyst showed good catalytic activity in the direct synthesis of H₂O₂ at atmospheric pressure, indicating that Pd catalyst supported on N-doped porous carbon has a promising research prospect. In particular, it was also shown that the ultrasonic-assisted-microwave quick synthesis method and NPCS support with high specific surface area and abundant mixed micro-mesoporous pore structure synergically improved the catalytic activity of Pd/NPCs catalyst.

4. Conclusions

In this work, we used mono-disperse, uniform-size and N-doped porous carbon sphere named as NPCS as a support to investigate the synthesis methods, temperature, reaction time, and Pd loading amount on the catalytic performance of Pd/NPCs catalysts for direct synthesis of hydrogen peroxide at ambient pressure. The results revealed that the ultrasonic-assisted microwave rapid synthesis method enabled the rapid and efficient synthesis of Pd/NPCs catalysts compared to other synthesis methods. The Pd/NPCs(W) catalysts exhibited favorable

characteristics, including uniform loading, small particle size, and narrow size distribution, with the Pd(111) crystal plane as the predominant surface structure. Furthermore, it was found that adjusting the Pd loading amount could alter the surface Pd⁰/Pd²⁺ ratio of Pd nanoparticles, thereby influencing the catalytic performance of Pd/NPCs(W) catalysts. Additionally, the N-doping, high specific surface area, and rich mixed mesoporous structure of the NPCS support further enhanced the transport and diffusion properties of Pd/NPCs catalysts. This facilitated the adsorption of reactants H₂ and O₂ on Pd active sites and the timely desorption of generated H₂O₂ into the reaction solution, effectively suppressing hydrogenation and decomposition side reactions caused by O-O bond cleavage and improving H₂O₂ selectivity. Consequently, at ambient pressure, the hydrogen peroxide productivity and selectivity of Pd_{0.3}/NPCs(W) were up to 219 mol_{H₂O₂}·kg_{cat}⁻¹·h⁻¹ and 76.7 %, respectively. This study provides a new synthesis strategy for designing high-performance Pd-based catalysts.

CRedit authorship contribution statement

Yongyong Shi: Formal analysis, Investigation, Methodology, Writing – original draft, Writing – review & editing. **Donghai Jiang:** Data curation, Investigation, Methodology. **Liming Zhou:** Data curation. **Jingyun Zhao:** Data curation. **Jun Ma:** Funding acquisition. **Qian Lin:** Funding acquisition, Resources, Supervision, Writing – review & editing. **Hongyan Pan:** Funding acquisition, Resources, Supervision.

Declaration of Competing Interest

The authors declare that they have no known competing financial interests or personal relationships that could have appeared to influence the work reported in this paper.

Acknowledgments

This work was financially supported by National Natural Science Foundation of China (Grant No.22068009), National Natural Science Foundation of China (Grant No.22262006), National Science Basic Research Program of Guizhou Province

(Grant No.ZK[2022]088), and Cultivation Project of Guizhou University (Grant No. [2020]38).

Appendix A. Supplementary data

Supplementary data to this article can be found online at <https://doi.org/10.1016/j.arabjc.2023.105100>.

References

- Abate, S., Arrigo, R., Schuster, M.E., et al, 2010. Pd nanoparticles supported on N-doped nanocarbon for the direct synthesis of H₂O₂ from H₂ and O₂. *Catal. Today* 157, 280–285. <https://doi.org/10.1016/j.cattod.2010.01.027>.
- Abate, S., Freni, M., Arrigo, R., et al, 2013. On the Nature of Selective Palladium-Based Nanoparticles on Nitrogen-Doped Carbon Nanotubes for the Direct Synthesis of H₂O₂. *ChemCatChem* 5, 1899–1905. <https://doi.org/10.1002/cctc.201200914>.
- Agarwal, N., Freakley, S.J., McVicker, R.U., et al, 2017. Aqueous Au-Pd colloids catalyze selective CH₄ oxidation to CH₃OH with O₂ under mild conditions. *Science* 358, 223–227. <https://doi.org/10.1126/science.aan6515>.
- Ao, C., Tian, P.F., Ouyang, L.K., et al, 2016. Dispersing Pd nanoparticles on N-doped TiO₂: a highly selective catalyst for H₂O₂ synthesis. *Cat. Sci. Technol.* 6, 5060–5068. <https://doi.org/10.1039/c5cy02275d>.
- Arrigo, R., Schuster, M.E., Abate, S., et al, 2014. Dynamics of palladium on nanocarbon in the direct synthesis of H₂O₂. *Chem. Sus. Chem.* 7, 179–194. <https://doi.org/10.1002/cssc.201300616>.
- Arrigo, R., Schuster, M.E., Abate, S., et al, 2016. Pd Supported on Carbon Nitride Boosts the Direct Hydrogen Peroxide Synthesis. *ACS Catal.* 6, 6959–6966. <https://doi.org/10.1021/acscatal.6b01889>.
- Cai, J.T., Chen, T., Cui, L., et al, 2020. A three-dimensional and porous bi-nanospheres electrocatalytic system constructed by in situ generation of Ru nanoclusters inside and outside polydopamine nanoparticles for highly efficient hydrogen evolution reaction. *Int. J. Hydrogen Energy* 45, 6592–6603. <https://doi.org/10.1016/j.ijhydene.2020.01.020>.
- Campos-Martin, J.M., Blanco-Brieva, G., Fierro, J.L., 2006. Hydrogen peroxide synthesis: an outlook beyond the anthraquinone process. *Angew Chem Int Ed Engl.* 45, 6962–6984. <https://doi.org/10.1002/anie.200503779>.
- Chang, Q., Zhang, P., Mostaghimi, A.H.B., et al, 2020. Promoting H₂O₂ production via 2-electron oxygen reduction by coordinating partially oxidized Pd with defect carbon. *Nat Commun.* 11, 2178. <https://doi.org/10.1038/s41467-020-15843-3>.
- Chen, L., Medlin, J.W., Grönbeck, H., 2021. On the Reaction Mechanism of Direct H₂O₂ Formation over Pd Catalysts. *ACS Catal.* 11, 2735–2745. <https://doi.org/10.1021/acscatal.0c05548>.
- Chen, Z., Pan, H., Lin, Q., et al, 2017. The modification of Pd core-silica shell catalysts by functional molecules (KBr, CTAB, SC) and their application to the direct synthesis of hydrogen peroxide from hydrogen and oxygen. *Cat. Sci. Technol.* 7, 1415–1422. <https://doi.org/10.1039/c7cy00105c>.
- Choudhary, V.R., Samanta, C., Choudhary, T.V., 2006. Direct oxidation of H₂ to H₂O₂ over Pd-based catalysts: Influence of oxidation state, support and metal additives. *Appl. Catal. A* 308, 128–133. <https://doi.org/10.1016/j.apcata.2006.04.010>.
- Choudhary, V.R., Samanta, C., Choudhary, T.V., 2006. Factors influencing decomposition of H₂O₂ over supported Pd catalyst in aqueous medium. *J. Mol. Catal. A Chem.* 260, 115–120. <https://doi.org/10.1016/j.molcata.2006.07.009>.
- Choudhary, V.R., Samanta, C., Jana, P., 2007. Formation from direct oxidation of H₂ and destruction by decomposition/hydrogenation of H₂O₂ over Pd/C catalyst in aqueous medium containing different acids and halide anions. *Appl. Catal. A* 317, 234–243. <https://doi.org/10.1016/j.apcata.2006.10.022>.
- Ciriminna, R., Albanese, L., Meneguzzo, F., et al, 2016. Hydrogen Peroxide: A Key Chemical for Today's Sustainable Development. *ChemSusChem* 9, 3374–3381. <https://doi.org/10.1002/cssc.201600895>.
- Cuong, D.V., Wu, P.C., Liu, N.L., et al, 2020. Hierarchical porous carbon derived from activated biochar as an eco-friendly electrode for the electrosorption of inorganic ions. *Sep. Purif. Technol.* 242. <https://doi.org/10.1016/j.seppur.2020.116813>.
- Cuong, D.V., Matsagar, B.M., Lee, M.S., et al, 2021. A critical review on biochar-based engineered hierarchical porous carbon for capacitive charge storage. *Renew. Sustain. Energy Rev.* 145. <https://doi.org/10.1016/j.rser.2021.111029>.
- Deng, J., Xiong, T.Y., Xu, F., et al, 2015. Inspired by bread leavening: one-pot synthesis of hierarchically porous carbon for supercapacitors. *Green Chem.* 17, 4053–4060. <https://doi.org/10.1039/c5gc00523j>.
- Ding, D.D., Xu, X.Y., Tian, P.F., et al, 2018. Promotional effects of Sb on Pd-based catalysts for the direct synthesis of hydrogen peroxide at ambient pressure. *Chin. J. Catal.* 39, 673–681. [https://doi.org/10.1016/S1872-2067\(18\)63031-1](https://doi.org/10.1016/S1872-2067(18)63031-1).
- Edwards, J. K., B. Solsona, E. N. N, et al., 2009. Switching off hydrogen peroxide hydrogenation in the direct synthesis process. *Science*. 323, 1037-1041. <https://doi.org/10.1126/science.1168980>.
- Edwards, J.K., Thomas, A., Solsona, B.E., et al, 2007. Comparison of supports for the direct synthesis of hydrogen peroxide from H₂ and O₂ using Au–Pd catalysts. *Catal. Today* 122, 397–402. <https://doi.org/10.1016/j.cattod.2007.01.046>.
- Edwards, J.K., Thomas, A., Carley, A.F., et al, 2008. Au–Pd supported nanocrystals as catalysts for the direct synthesis of hydrogen peroxide from H₂ and O₂. *Green Chem.* 10, 388–394. <https://doi.org/10.1039/b714553p>.
- Edwards, J.K., Freakley, S.J., Carley, A.F., et al, 2014. Strategies for designing supported gold-palladium bimetallic catalysts for the direct synthesis of hydrogen peroxide. *Acc Chem Res.* 47, 845–854. <https://doi.org/10.1021/ar400177c>.
- Edwards, J.K., Freakley, S.J., Lewis, R.J., et al, 2015. Advances in the direct synthesis of hydrogen peroxide from hydrogen and oxygen. *Catal. Today* 248, 3–9. <https://doi.org/10.1016/j.cattod.2014.03.011>.
- Freakley, S.J., Piccinini, M., Edwards, J.K., et al, 2013. Effect of Reaction Conditions on the Direct Synthesis of Hydrogen Peroxide with a AuPd/TiO₂ Catalyst in a Flow Reactor. *ACS Catal.* 3, 487–501. <https://doi.org/10.1021/cs400004y>.
- Gao, G.H., Tian, Y.N., Gong, X.X., et al, 2020. Advances in the production technology of hydrogen peroxide. *Chin. J. Catal.* 41, 1039–1047. [https://doi.org/10.1016/S1872-2067\(20\)63562-8](https://doi.org/10.1016/S1872-2067(20)63562-8).
- García, T., Agouram, S., Dejoj, A., et al, 2015. Enhanced H₂O₂ production over Au-rich bimetallic Au–Pd nanoparticles on ordered mesoporous carbons. *Catal. Today* 248, 48–57. <https://doi.org/10.1016/j.cattod.2014.03.039>.
- García-Serna, J., Moreno, T., Biasi, P., et al, 2014. Engineering in direct synthesis of hydrogen peroxide: targets, reactors and guidelines for operational conditions. *Green Chem.* 16. <https://doi.org/10.1039/c3gc41600c>.
- Gong, Y., Xie, L., Li, H., et al, 2014. Sustainable and scalable production of monodisperse and highly uniform colloidal carbonaceous spheres using sodium polyacrylate as the dispersant. *Chem Commun (Camb).* 50, 12633–12636. <https://doi.org/10.1039/c4cc04998e>.
- Guo, L., Guo, Z., Liang, J., et al, 2022. Quick microwave assembling nitrogen-regulated graphene supported iron nanoparticles for Fischer-Tropsch synthesis. *Chem. Eng. J.* 429. <https://doi.org/10.1016/j.cej.2021.132063>.
- Han, G.H., Seo, M.G., Cho, Y.H., et al, 2017. Highly dispersed Pd catalysts prepared by a sonochemical method for the direct

- synthesis of hydrogen peroxide. *Mol. Catal.* 429, 43–50. <https://doi.org/10.1016/j.molcata.2016.12.003>.
- Han, G.H., Lee, S.H., Hwang, S.Y., et al, 2021. Advanced Development Strategy of Nano Catalyst and DFT Calculations for Direct Synthesis of Hydrogen Peroxide. *Adv Energy Mater* 11. <https://doi.org/10.1002/aenm.202003121>.
- Hu, B.Z., Deng, W.P., Li, R.S., et al, 2014. Carbon-supported palladium catalysts for the direct synthesis of hydrogen peroxide from hydrogen and oxygen. *J. Catal.* 319, 15–26. <https://doi.org/10.1016/j.jcat.2014.08.001>.
- Huang, W., Zhang, S., Tang, Y., et al, 2016. Low-Temperature Transformation of Methane to Methanol on Pd1 O4 Single Sites Anchored on the Internal Surface of Microporous Silicate. *Angew Chem Int Ed Engl.* 55, 13441–13445. <https://doi.org/10.1002/anie.201604708>.
- Ji, X., Chen, D.D., Peng, L., et al, 2021. Sustainable direct H₂O₂ synthesis over Pd catalyst supported on mesoporous carbon: The effect of surface nitrogen functionality. *Catal. Today* 376, 1–8. <https://doi.org/10.1016/j.cattod.2020.12.036>.
- Jia, W., Zhang, J., Le, F., et al, 2020. Dual-nitrogen-source strategy for N-doped graphitic layer-wrapped metal carbide toward efficient oxygen reduction reaction. *J Colloid Interface Sci.* 567, 165–170. <https://doi.org/10.1016/j.jcis.2020.02.005>.
- Jiang, D., Shi, Y., Zhou, L., et al, 2023. Promotional effect of nitrogen-doped and pore structure for the direct synthesis of hydrogen peroxide from hydrogen and oxygen by Pd/C catalyst at ambient pressure. *Arab. J. Chem.* 16. <https://doi.org/10.1016/j.arabj.2022.104452>.
- Jin, Z., Wang, L., Zuidema, E., et al, 2020. Hydrophobic zeolite modification for in situ peroxide formation in methane oxidation to methanol. *Science* 367, 193–197. <https://doi.org/10.1126/science.aaw1108>.
- Lari, G.M., Puertolas, B., Shahrokhi, M., et al, 2017. Hybrid Palladium Nanoparticles for Direct Hydrogen Peroxide Synthesis: The Key Role of the Ligand. *Angew Chem Int Ed Engl.* 56, 1775–1779. <https://doi.org/10.1002/anie.201610552>.
- Lee, S., Jeong, H., Chung, Y.M., 2018. Direct synthesis of hydrogen peroxide over Pd/C catalyst prepared by selective adsorption deposition method. *J. Catal.* 365, 125–137. <https://doi.org/10.1016/j.jcat.2018.06.024>.
- Lee, J.W., Kim, J.K., Kang, T.H., et al, 2017. Direct synthesis of hydrogen peroxide from hydrogen and oxygen over palladium catalyst supported on heteropolyacid-containing ordered mesoporous carbon. *Catal. Today* 293, 49–55. <https://doi.org/10.1016/j.cattod.2016.10.008>.
- Lewis, R.J., Hutchings, G.J., 2018. Recent Advances in the Direct Synthesis of H₂O₂. *ChemCatChem* 11, 298–308. <https://doi.org/10.1002/cctc.201801435>.
- Lewis, R.J., Ntainjua, E.N., Morgan, D.J., et al, 2021. Improving the performance of Pd based catalysts for the direct synthesis of hydrogen peroxide via acid incorporation during catalyst synthesis. *Catal. Commun.* 161. <https://doi.org/10.1016/j.catcom.2021.106358>.
- Lewis, R.J., Ueura, K., Liu, X., et al, 2022. Highly efficient catalytic production of oximes from ketones using in situ-generated H₂O₂. *Science* 376, 615–620. <https://doi.org/10.1126/science.abl4822>.
- Li, J., Ishihara, T., Yoshizawa, K., 2011a. Theoretical Revisit of the Direct Synthesis of H₂O₂ on Pd and Au@Pd Surfaces: A Comprehensive Mechanistic Study. *J Phys Chem C.* 115, 25359–25367. <https://doi.org/10.1021/jp208118e>.
- Li, J., Staykov, A., Ishihara, T., et al, 2011b. Theoretical Study of the Decomposition and Hydrogenation of H₂O₂ on Pd and Au@Pd Surfaces: Understanding toward High Selectivity of H₂O₂ Synthesis. *J Phys Chem C.* 115, 7392–7398. <https://doi.org/10.1021/jp1070456>.
- Liu, Q., Bauer, J.C., Schaak, R.E., et al, 2008. Supported palladium nanoparticles: an efficient catalyst for the direct formation of H₂O₂ from H₂ and O₂. *Angew Chem Int Ed Engl.* 47, 6221–6224. <https://doi.org/10.1002/anie.200801517>.
- Liu, P., Lin, Q., Pan, H., et al, 2019. Direct synthesis of hydrogen peroxide from hydrogen and oxygen over yolk-shell nanocatalyst Pd@HCS with controlled Pd nanoparticle size. *J. Catal.* 377, 511–523. <https://doi.org/10.1016/j.jcat.2019.07.044>.
- Ma, L., Gao, Q., Tian, W., et al, 2018. A Large-Sized Reduced Graphene Oxide with Low Charge-Transfer Resistance as a High-Performance Electrode for a Nonflammable High-Temperature Stable Ionic-Liquid-Based Supercapacitor. *ChemSusChem* 11, 4026–4032. <https://doi.org/10.1002/cssc.201801968>.
- Mao, D., Jia, M., Qiu, J., et al, 2019. N-Doped Porous Carbon Supported Au Nanoparticles for Benzyl Alcohol Oxidation. *Catal. Lett.* 150, 74–81. <https://doi.org/10.1007/s10562-019-02949-7>.
- Mao, J., Niu, D., Jiang, N., et al, 2020. Rational design of high nitrogen-doped and core-shell/mesoporous carbon nanospheres with high rate capability and cycling longevity for pseudocapacitive sodium storage. *J. Mater. Chem. A* 8, 9768–9775. <https://doi.org/10.1039/d0ta03229h>.
- Menegazzo, F., Signoretto, M., Frison, G., et al, 2012. When high metal dispersion has a detrimental effect: Hydrogen peroxide direct synthesis under very mild and nonexplosive conditions catalyzed by Pd supported on silica. *J. Catal.* 290, 143–150. <https://doi.org/10.1016/j.jcat.2012.03.010>.
- Ntainjua, N.E., Edwards, J.K., Carley, A.F., et al, 2008. The role of the support in achieving high selectivity in the direct formation of hydrogen peroxide. *Green Chem.* 10. <https://doi.org/10.1039/b809881f>.
- Piccinini, M., Edwards, J.K., Moulijn, J.A., et al, 2012. Influence of reaction conditions on the direct synthesis of hydrogen peroxide over AuPd/carbon catalysts. *Cat. Sci. Technol.* 2, 1908–1913. <https://doi.org/10.1039/c2cy20282d>.
- Pu, C., Zhang, J., Chang, G.G., et al, 2020. Nitrogen precursor-mediated construction of N-doped hierarchically porous carbon-supported Pd catalysts with controllable morphology and composition. *Carbon* 159, 451–460. <https://doi.org/10.1016/j.carbon.2019.12.058>.
- Rankin, R.B., Greeley, J., 2012. Trends in Selective Hydrogen Peroxide Production on Transition Metal Surfaces from First Principles. *ACS Catal.* 2, 2664–2672. <https://doi.org/10.1021/cs3003337>.
- Samanta, C., 2008. Direct synthesis of hydrogen peroxide from hydrogen and oxygen: An overview of recent developments in the process. *Appl Catal a-Gen.* 350, 133–149. <https://doi.org/10.1016/j.apcata.2008.07.043>.
- Seo, M.-G., Kim, H.J., Han, S.S., et al, 2016. Direct Synthesis of Hydrogen Peroxide from Hydrogen and Oxygen Using Tailored Pd Nanocatalysts: A Review of Recent Findings. *Catal. Surv. Asia* 21, 1–12. <https://doi.org/10.1007/s10563-016-9221-y>.
- Shi, C., Hu, L., Guo, K., et al, 2017. Highly Porous Carbon with Graphene Nanoplatelet Microstructure Derived from Biomass Waste for High-Performance Supercapacitors in Universal Electrolyte. *Advanced Sustainable Systems.* 1. <https://doi.org/10.1002/adsu.201600011>.
- Staykov, A., Kamachi, T., Ishihara, T., et al, 2008. Theoretical Study of the Direct Synthesis of H₂O₂ on Pd and Pd/Au Surfaces. *J Phys Chem C.* 112, 19501–19505. <https://doi.org/10.1021/jp803021n>.
- Thuy Vu, H.T., Nam Vo, V.L., Chung, Y.-M., 2020. Geometric, electronic, and synergistic effect in the sulfonated carbon-supported Pd catalysts for the direct synthesis of hydrogen peroxide. *Appl. Catal. A* 607. <https://doi.org/10.1016/j.apcata.2020.117867>.
- Tian, P.F., Ding, D.D., Sun, Y., et al, 2019. Theoretical study of size effects on the direct synthesis of hydrogen peroxide over palladium catalysts. *J. Catal.* 369, 95–104. <https://doi.org/10.1016/j.jcat.2018.10.029>.
- Tian, P., Ouyang, L., Xu, X., et al, 2013. Density functional theory study of direct synthesis of H₂O₂ from H₂ and O₂ on Pd(111), Pd

- (100), and Pd(110) surfaces. *Chin. J. Catal.* 34, 1002–1012. [https://doi.org/10.1016/s1872-2067\(12\)60537-3](https://doi.org/10.1016/s1872-2067(12)60537-3).
- Tian, P., Ouyang, L., Xu, X., et al, 2017. The origin of palladium particle size effects in the direct synthesis of H₂O₂: Is smaller better? *J. Catal.* 349, 30–40. <https://doi.org/10.1016/j.jcat.2016.12.004>.
- Wang, X., Pan, H., Lin, Q., et al, 2019. One-Step Synthesis of Nitrogen-Doped Hydrophilic Mesoporous Carbons from Chitosan-Based Triconstituent System for Drug Release. *Nanoscale Res Lett.* 14, 259. <https://doi.org/10.1186/s11671-019-3075-y>.
- Wang, Y., Zhang, X., Qiu, D., et al, 2018. Ultrasonic assisted microwave synthesis of poly (Chitosan-co-gelatin)/polyvinyl pyrrolidone IPN hydrogel. *Ultrason Sonochem.* 40, 714–719. <https://doi.org/10.1016/j.ultsonch.2017.08.003>.
- Wu, Y.H., Gao, Z.X., Feng, Y.R., et al, 2021. Harnessing selective and durable electrosynthesis of H₂O₂ over dual-defective yolk-shell carbon nanosphere toward on-site pollutant degradation. *Applied Catalysis B-Environmental.* 298. <https://doi.org/10.1016/j.apcatb.2021.120572>.
- Xie, L., Li, X.F., Deng, J., et al, 2018. Sustainable and scalable synthesis of monodisperse carbon nanospheres and their derived superstructures. *Green Chem.* 20, 4596–4601. <https://doi.org/10.1039/c8gc02196a>.
- Yook, S., Kwon, H.C., Kim, Y.-G., et al, 2016. Significant Roles of Carbon Pore and Surface Structure in AuPd/C Catalyst for Achieving High Chemoselectivity in Direct Hydrogen Peroxide Synthesis. *ACS Sustain. Chem. Eng.* 5, 1208–1216. <https://doi.org/10.1021/acssuschemeng.6b02595>.
- Yuan, Y., Zhao, H., Xu, W., et al, 2022. Noble metal aerogels rapidly synthesized by ultrasound for electrocatalytic reaction. *Chin. Chem. Lett.* 33, 2021–2025. <https://doi.org/10.1016/j.cclet.2021.09.104>.
- Zhang, R.N., Gu, X., Liu, Y.H., et al, 2020. Hydrophilic nano-porous carbon derived from egg whites for highly efficient capacitive deionization. *Appl. Surf. Sci.* 512. <https://doi.org/10.1016/j.apsusc.2020.145740>.
- Zhang, M.J., Luo, Y.B., Wu, D.F., et al, 2021a. Promoter role of tungsten in W-Pd/Al₂O₃ catalyst for direct synthesis of H₂O₂: Modification of Pd/PdO ratio. *Appl Catal a-Gen.* 628.
- Zhang, Z., Wen, G., Luo, D., et al, 2021b. “Two Ships in a Bottle” Design for Zn-Ag-O Catalyst Enabling Selective and Long-Lasting CO₂ Electroreduction. *J Am Chem Soc.* 143, 6855–6864. <https://doi.org/10.1021/jacs.0c12418>.
- Zhang, M.M., Xie, J.M., Sun, Q., et al, 2013. In situ synthesis of palladium nanoparticle on functionalized graphene sheets at improved performance for ethanol oxidation in alkaline media. *Electrochim. Acta* 111, 855–861. <https://doi.org/10.1016/j.electacta.2013.08.135>.
- Zhao, Y., Fan, D., Cao, S., et al, 2023. Visualization of biochar colloids transport and retention in two-dimensional porous media. *J. Hydrol.* 619. <https://doi.org/10.1016/j.jhydrol.2023.129266>.
- Zhou, T., Wang, L.J., Zheng, S.Q., et al, 2018. Self-assembled 3D flower-like hierarchical Ti-doped Cu₃SbSe₄ microspheres with ultralow thermal conductivity and high zT. *Nano Energy* 49, 221–229. <https://doi.org/10.1016/j.nanoen.2018.04.035>.
- Zhu, Y.Y., Chen, M.M., Zhang, Y., et al, 2018. A biomass-derived nitrogen-doped porous carbon for high-energy supercapacitor. *Carbon* 140, 404–412. <https://doi.org/10.1016/j.carbon.2018.09.009>.